NRL Report 6791

The Experimental Examination, by Means of Pulses, of Circumferential Waves on Aluminum Cylinders in Water

WERNER G. NEUBAUER

Physical Acoustics Branch
Acoustics Division

November 15, 1968

NAVAL RESEARCH LABORATORY
Washington, D.C.

This document has been approved for public release and sale; its distribution is unlimited.

This report is based on the work leading to a dissertation submitted to the Catholic University of America in partial fulfillment for the degree of Doctor of Philosophy conferred October 7, 1968.

TABLE OF CONTENTS

	Page
Abstract	ii
Problem Status	ii
Authorization	ii
INTRODUCTION	1
EXPERIMENTAL RESULTS	7
I - THE "FRANZ TYPE" OR "CREEPING" WAVE	7
II - THE "RAYLEIGH TYPE" WAVE	21
III - A THIRD CIRCUMFERENTIAL WAVE	33
IV - THE TOTAL DIFFRACTED FIELD	41
V - A DISCUSSION OF EXPERIMENTAL RESULTS AND COMPARISON WITH THE CALCULATIONS OF UGINČIUS	44
VI - CONCLUSIONS	52
ACKNOWLEDGEMENTS	54
REFERENCES	55
APPENDIX A: The Experimental Apparatus and Procedures	57
APPENDIX B: The Schlieren Visualization of Waves	64

ABSTRACT

Three types of waves which contribute to the total acoustic diffracted field of an aluminum cylinder in water are isolated by generating each wave to the exclusion of the other two. Observations of circumferential propagation speed and attenuation are made. The "Franz type" or "creeping" wave is generated separately on the outside of aluminum cylinders with ka ranging from 54 to 1008. The circumferential-wave speed is found to be 1% less than that of the free water-borne wave in agreement with the theory for a rigid cylinder. The attenuation of these waves on aluminum cylinders is significantly less than the theory for the rigid cylinder predicts. Another circumferential wave with approximately a 30° incidence and emergence angle is found to propagate on the inside of the curved boundary. This wave has an attenuation ranging between 0.10 and 0.18 Np/rad and has a speed of 2.5 times that of the free water-borne wave. This is classified as a "Rayleigh type" wave. A third wave is observed which is similar to the wave generated at 30° incidence but has a 15° incidence and emergence angle. The attenuation is between 0.08 and 0.14 Np/rad and has a speed of 6.5 times that of the free water-borne wave. Experimental measurements of differential-scattering cross section are compared to those calculated by means of the creeping wave formulation.

PROBLEM STATUS

This is an interim report on the problem; work is continuing.

AUTHORIZATION

NRL Problem 81S01-04

Project RF 05-511-401-5252

Manuscript submitted October 14, 1968.

INTRODUCTION

Numerous experimenters have observed effects of diffraction which they have been compelled to explain in terms of waves which are presumed to propagate along the curved surface of the diffracting object. The theoretical formulation of circumferentially traveling waves stemming from the Sommerfeld-Watson[1] transformation originated with interest in the propagation of radio waves around the earth's surface by van der Pol and Bremmer.[2] Later Franz and Deppermann[3] treated the case of circumferentially traveling waves on a cylinder, apparently named the "creeping wave" (Kriechwelle) and also gave the first comparison of experimentally measured values for backscattering of electromagnetic waves and theoretical results utilizing the creeping wave formulation. The consideration of creeping waves in acoustic phenomena was first discussed by Freedman[4] for the case of backscattering. The experimental observation by Barnard and McKinney[5] of a periodic structure following and lasting much longer than the acoustic pulse incident on elastic cylinders, at the time seemed reasonably explained by them as the observation of "creeping waves". This conclusion was further supported by the observation of apparent circumferentially traveling pulses in a non-back-scattering direction. These same types of pulses (waves) were later further studied by Horton, et al.[6], Diercks, et al.[7], Goldsberry[8], and Mechler[9], whose results showed these waves to have properties not related to the waves of Franz but rather to be related to elastic properties of the boundary. Goodman, et al.[10] isolated an elastic Rayleigh-type wave of this same kind on aluminum cylinders in water. Waves probably having circumferential paths were also present in studies of spherical shells by Hickling[11] but were not recognized as such since the classical orthogonal-function solution did not indicate separate wave isolation. In the work presented here, the "Franz type" or creeping wave is isolated and its properties are measured and its radiated effect is observed. In addition, two types of elastic circumferential boundary waves generated at different characteristic incidence angles are isolated, measured and their radiation observed. Creeping wave formulation has been extended to consideration of the use of sound pulses to study circumferential waves by Überall, et al.[12]. Doolittle, et al.[13] treated the scattering by elastic cylinders, and Uginčius and Überall[14] treated the scattering by elastic cylindrical shells. The last three references have been the motivation for this experimental study whose major significance is the positive identification of three different and separate waves by two independent experimental methods. Generally, specific experiments have not been designed

to relate to specific theoretical computation incorporating into it the appropriate achievable or measured parameters. Theory has proceeded largely on limiting cases such as either acoustically infinitely soft or rigid boundary conditions. Elastic cases have been worked out on the basis of material constants extracted from handbooks and mainly for small values of ka.

At least two types of circumferentially traveling waves are known to exist on curved surfaces. One, the "Franz type" or "creeping wave" is primarily related to the geometry or curvature of the diffracting object and is slightly affected by the material of the boundary. It is present in both limiting cases of infinitely soft or rigid curved boundaries. The other, which some prefer to call a refracted circumferential wave, is primarily related to the material of the diffracting body and is less affected by the boundary curvature. It is not present in the limiting cases of either acoustically soft or acoustically rigid boundary conditions.

There is a single physically observable composite result when an incident wave interacts with a body which it encounters in its progress. The total diffraction by structured bodies is a result of several physical processes or mechanisms. The reality and relative importance of the constituents of reflection and diffraction as they are interpreted from a specific theoretical approach are of interest. All theories which formulate the problem with the same boundary conditions may be reasonably expected to contain the same elements or mechanisms. This seems to be the case with the creeping wave formulation, the methods of Viktorov[15] and Brekhovskikh[16], and the classical orthogonal-function-series expansion[17]. The completeness of each of these formulations and the identification, and degree of importance, of types of waves or separate mechanisms, and how they may be most conveniently computed or observed is not yet adequately known.

Experiments designed to examine the structure of the diffracted field have in general not been guided by specific theory or computed results based on the experimental parameters. Three notable exceptions are available. Faran[18] treated the net diffracted field of cylinders and spheres guided by the classical orthogonal-function solution. Prior to the day of the ubiquitous digital computer, Faran computed total diffracted fields and found favorable experimental comparison with cases that he computed. Willie[19] later treated diffraction by cylinders and spheres and careful measurements showed the applicability of the creeping wave formulation, for steady state signals, using only the largest creeping wave. He found agreement between total diffraction calculations and experiments for the limiting cases of infinitely soft and hard boundary conditions. The existence and

properties of the creeping wave were implied by their interference in the diffraction region of the spheres and cylinders.

Bunney[20] has recently produced experimental results which, for the first time, directly identify and measure specific isolated waves which contribute to the total diffraction by an elastic cylinder. Also, Bunney made a direct comparison of the theoretical calculation of a specific theory, after Viktorov[15], and extended by Grace and Goodman[21] of the surface wave behavior and experimental observation. The theory of Viktorov and Grace and Goodman was particularly amenable to the isolation of the circumferential "Rayleigh type" wave which Bunney observed.

The creeping wave formulation, with its advantage of rapid convergence, is of special interest to this work. The work of Überall, et al., especially the computations of Uginčius, provide a basis for the identification of separate waves which emerge from the creeping wave formulation. The calculation reveals essentially two types of poles in the complex plane which are labeled in Fig. 1(a) as a series of F poles and a series of R poles.

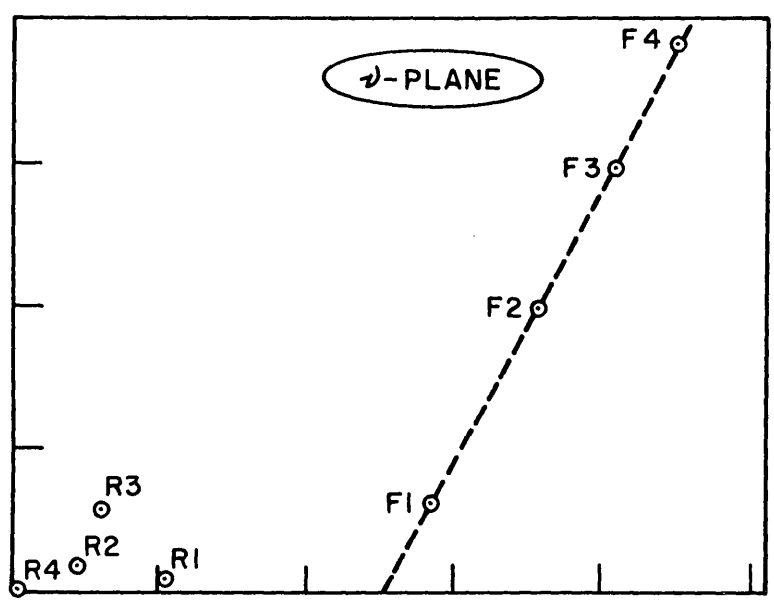

Fig. 1(a)—The positions of Franz and Rayleigh-type poles in the complex ν-plane for an aluminum shell with inner-to-outer radius ratio (b/a) of 0.05, for ka = 5.

In the absence of a straightforward manner of locating the poles in the complex ν-plane, Uginčius searched that plane for the poles which existed for various values of the parameter ka. He plotted the R-type poles in a "reduced" ν/ka-plane as seen in Fig. 1(b) to show the limiting behavior of the pole locus with increasing ka. Having calculated up to values of ka of 80 and 90, he concluded that the R1 pole approached the Rayleigh limit shown which is the value for the Rayleigh wave on an infinite aluminum plane bounded by water.[21] The R2 and higher Rn poles, he conjectured, approached the Stoneley limit.[21] Uginčius takes only the poles in the first quadrant to be physically

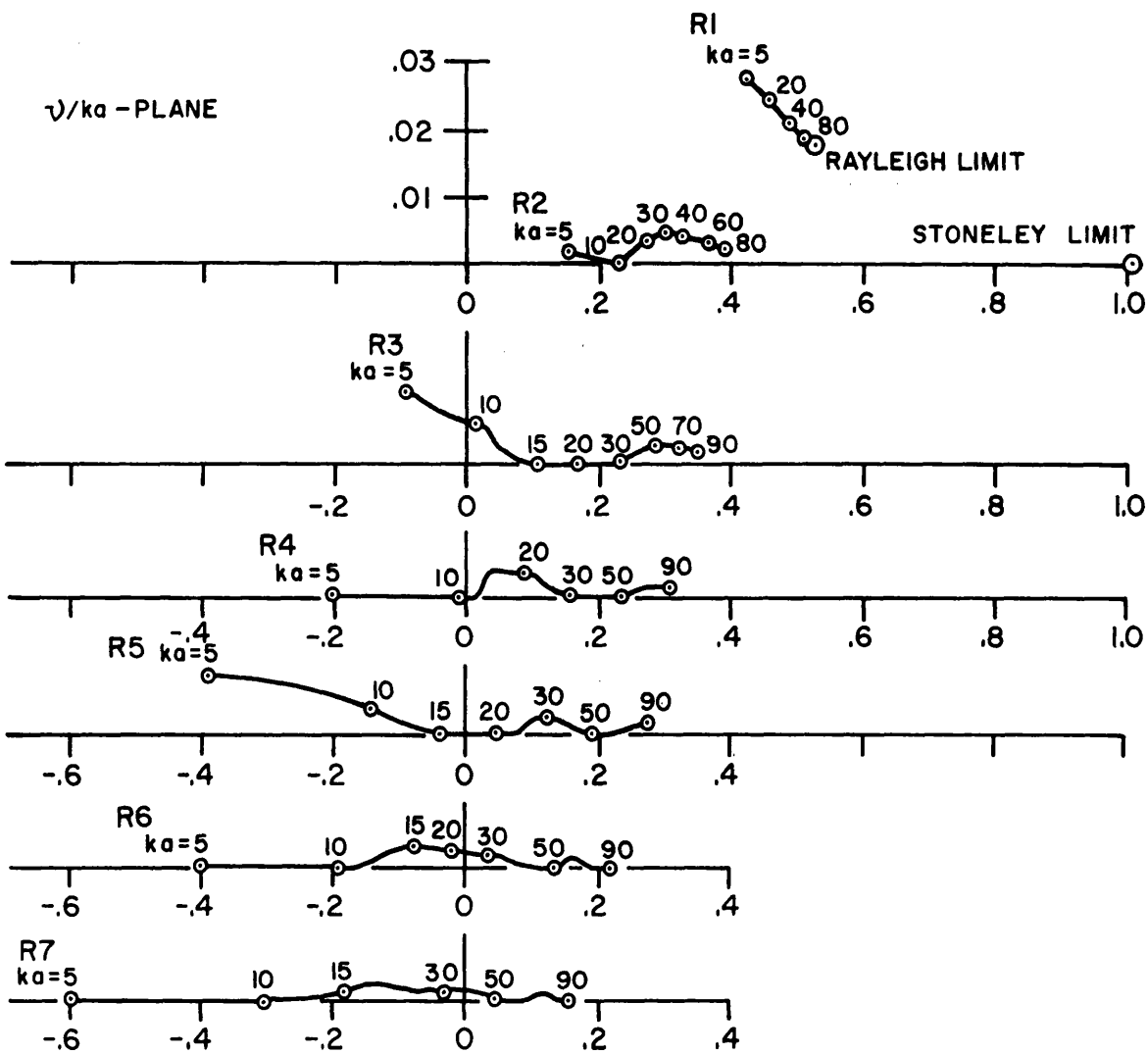

Fig. 1(b)–First seven Rayleigh zeroes in the reduced plane ν/ka vs. ka for a solid aluminum cylinder in water.

meaningful or interpretable poles, corresponding to real but attenuated or measurable waves. For a low ka of 5, only the R1 and R2 poles are in the first quadrant. As ka increases, a greater number of separately identifiable poles move into the first quadrant from the second quadrant. The real part of any pole position or complex value of ν, is inversely proportional to the velocity of a circumferential wave whose properties that pole describes. The imaginary part of ν is directly proportional to the attenuation of the circumferential wave. Thus Fig. 1(b) allows the following interpretation:

(a) For values of ka above 80, the R1 wave is nearly at the Rayleigh limit, i.e., the attenuation and velocity can be expected to change very little as $ka \to \infty$.

(b) The R1 wave has significantly higher attenuation than the higher order R waves.

(c) For lower ka, fewer orders of R waves exist.

(d) There are values of ka for R2 and higher orders which have negligible attenuation (imaginary part of ν). This indicates no or insignificant loss of energy by these waves and, therefore, they must not radiate and will not be detectable in the field surrounding the cylinder.

(e) Up to ka = 90, the higher order R waves all have a velocity higher than the R1 wave and if they exist at a given ka, higher order R waves have higher velocities than the lower R waves.

The F poles are those identified by Franz[22] for the completely soft or rigid cases of cylinders and spheres. The following description of the properties and behavior of the "Franz type" or "creeping" wave is consistent with both the theoretical computation of the F poles and their behavior, and the experimental observation of the wave (or waves) related to them. In this description, the use of a geometric ray is helpful to understanding by tracing the wave path, even though the concept is basically one of a wave structure. Such a mixture of concepts is not without precedence since Keller[23] discusses "diffracted rays" in describing diffraction within the shadow region of a curved surface. A ray incident along a tangent to the cross section of a cylinder causes a set of waves to be launched at the point of tangency which is propagated along the circumference of the cross section. Each member of the set corresponds to a member of the line of F poles in the complex ν-plane. For each wave component its propagation properties are related to the position of the pole; the wave velocity being inversely proportional to the real part of the complex value locating the pole and the attenuation being directly proportional to the imaginary part. The total wave packet (or waves) or set, therefore, contains seperate wave components each of which has a different speed and attenuation. The magnitude

of the contribution of any wave represented by a pole is the value of the residue at that pole. The major contribution to the net wave is related to the pole with the smallest imaginary part, i.e., having the least attenuation. A line drawn through the poles intersects the real axis at a value of approximately ka. As soon as a wave is launched at the point of tangency and propagated an incremental distance along the circumference, part of the wave is radiated into the shadow region again along a ray tangent to the cylinder cross section. The remainder of the wave continues to propagate along the circumference, constantly radiating into the shadow region. Thus the circumferential or boundary wave constantly loses energy into the region around the cylinder. If the attenuation is sufficiently low so that the amplitude of the circumferential wave is still large enough when the shadow boundary on the opposite side of the cylinder is reached, the wave will, of course, radiate into the so-called "lit region" and eventually constitute what is thought of as reflection. This will occur to a significant degree at relatively low ka (say ka = 10). At the present state of understanding, no more is known about the other types of circumferential waves than to classify them under a single category. One of these waves, discussed by Bunney, is called the "Rayleigh type" because its properties seem to approach the properties of the Rayleigh wave in the limiting case of $ka \to \infty$, i.e., the limit of a infinite-plane boundary separating a solid elastic medium from a vacuum. This is apparently the wave related to the pole in the complex ν-plane which Uginčius specified as R1. The remining Rn poles have not been related to any observations nor have any observations been related to these circumferential waves in other theories.

In the work to be presented, the Franz wave and the two different refracted waves are separately produced and examined by the selective insonification of the cylinder at specific incidence angles.

EXPERIMENTAL RESULTS

I – The "Franz Type" or "Creeping" Wave

The velocity and attenuation of the "Franz type" wave have been directly measured experimentally with a differential-path method. The diffracting aluminum cylinder in all measurements was immersed in water. The pulse used for the acoustic-pressure-pulse measurements was produced by imposing a step function on a lead-zirconate-titanate transducer resonant at one MHz. A description of the electronic and physical apparatus is given in Appendix A. Although the transducer was mounted in a circular faced housing, the active element was 2.54 cm square. Such a square radiator produces smaller side lobes than an equivalent circular source transducer. The acoustic pulse transmitted through the water in a free field is shown in Fig. 2. The width of the main

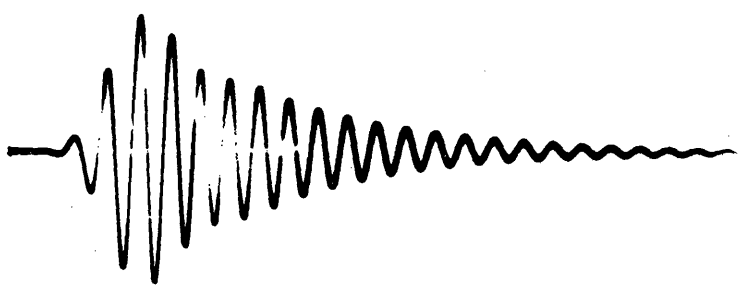

Fig. 2–The acoustic pulse received at position 1 in Fig. 3 in the absence of the cylinder.

lobe of the transducer is 12° with essentially no side lobes. The signal which issued at all angles beyond ±6° of the central axis of the transducer was 40 dB below the main lobe. The "Franz wave" is produced by impinging an acoustic wave at a point on the cylinder normal to one of the cylinder's elements along a tangent to the circular cross section of the cylinder. The configuration for the experimental arrangement for generating and measuring the properties of the "Franz type" wave is shown in Fig. 3. The line from the acoustic source to the cylinder represents the central ray of the source.

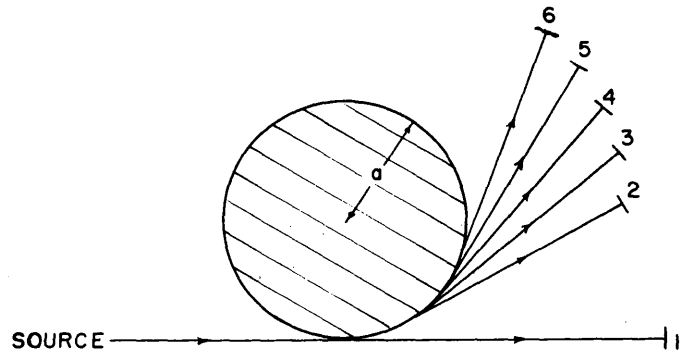

Fig. 3–Experimental configuration for observing and measuring the properties of the Franz wave on a solid cylinder.

Figure 4 shows the pulse which has been propagated along a circumferential path and then radiated tangentially to position 6 in Fig. 3. Although the pulses in Fig. 2 and Fig. 4 appear to have the same envelope, a double exposure of the two pulses shown in Fig. 5, equalized in amplitude at the first cycle of each, shows that the envelopes are actually slightly different. A change in pulse envelope in the course of propagation of the pulse can be attributable to dispersion caused by the medium in which the pulse is propagated, i.e., the Fourier components of the pulse are propagated with different velocities. In this case, the pulse shape change is caused by differential attenuation.

This creeping wave is a circumferential wave which propagates on the outside of the boundary. This was verified by placing an obstruction along one of the elements of the cylinder at a point on the circumference between the tangential incidence point and the tangential emergence point. The wave was thus completely stopped. It was interesting

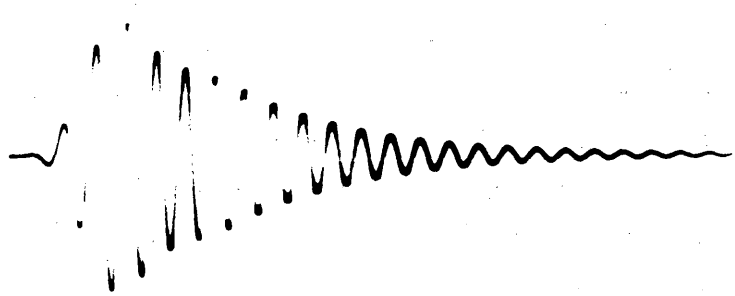

Fig. 4–The acoustic pulse received at position 6 in Fig. 3.

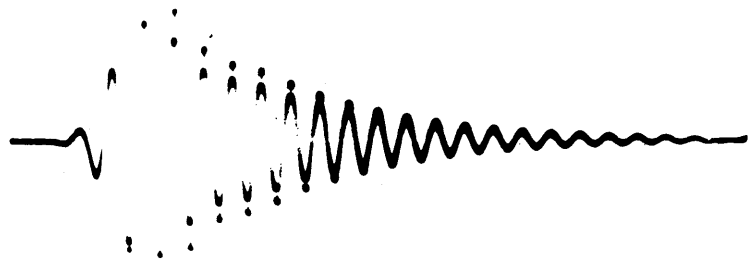

Fig. 5—Double exposure of the acoustic pulse received at positions 1 and 6 with equalized first cycles.

to notice that a slight opening of less than a wavelength between the obstruction and the cylinder's surface allowed a large part of the wave to pass.

The net creeping wave is launched at the tangential point of incidence. Each wave is related to a pole in the group of F poles of Fig. 1(a). Formulas for calculation of the position of poles located at ν_ℓ are given by Franz[22] for the case of the large rigid as well as the large soft cylinder. For the rigid cylinder,

$$\nu_\ell \approx ka + \left(\frac{ka}{6}\right)^{1/3} e^{i\pi/3}\, q_\ell - \left(\frac{6}{ka}\right)^{1/3} e^{-i\pi/3} \left(\frac{1}{10 q_\ell} + \frac{q_\ell^{\,2}}{180}\right). \tag{1}$$

The index $\ell = 1, 2, 3, \ldots$, where increasing ℓ is in the direction of increasing real and imaginary parts of ν_ℓ.

For the soft cylinder,

$$\bar{\nu}_\ell \approx ka + \left(\frac{ka}{6}\right)^{1/3} e^{i\pi/3}\, \bar{q}_\ell - \left(\frac{6}{ka}\right)^{1/3} e^{-i\pi/3} \left(\frac{\bar{q}_\ell^{\,2}}{180}\right). \tag{2}$$

In Eqs. 1 and 2, $\bar{q}_\ell$ and q_ℓ are the zeroes of the Airy integral

$$A(q) = \int_0^\infty \cos\,(t^3 - qt)\, dt$$

and $\dfrac{dA(q)}{dq}$ respectively.

Values of q_ℓ and $\bar{q}_\ell$ used to compute ν_ℓ and $\bar{\nu}_\ell$ for comparison with experimental measurements are given in Table I.

TABLE I

VALUES OF q_ℓ AND $\bar{q}_\ell$ USED FOR COMPUTATION OF ν_ℓ AND $\bar{\nu}_\ell$ FROM EQS. 1 AND 2 RESPECTIVELY.

ℓ	q_ℓ	$\bar{q}_\ell$
1	1.469354	3.372134
2	4.684712	5.895843
3	6.951786	7.962025
4	8.889027	9.788127
5	10.632519	11.457423

The circumferential-wave residue series for the case of a distant observation point is ultimately expressed in wave form by Uginčius and Überall as terms having the form

$$e^{i(\pm\nu_\ell\theta - \omega t)} = e^{-\mathrm{Im}(\nu_\ell)(\pm\theta)}\, e^{i[\pm\mathrm{Re}(\nu_\ell)\,\theta - \omega t]}, \tag{3}$$

i.e., a wave which decays at a rate of $\mathrm{Im}\nu_\ell$ expressed in Np/deg and having a propagation constant $\mathrm{Re}\nu_\ell/a$ in the direction $\pm\theta$.

The propagation constant is the ratio of the angular frequency to the wave phase velocity so,

$$\frac{\mathrm{Re}\nu_\ell}{a} = \frac{\omega}{c_c}$$

and

$$\frac{ka}{\mathrm{Re}\nu_\ell} = \frac{c_c}{c_w}. \tag{4}$$

Circumferential wave velocities (c_c) will be expressed in this form, normalized to the free-wave velocity (c_w) in the fluid external to the cylinder.

In summary: the circumferential wave traveling in either direction around the cylinder has a wave speed inversely proportional to $\mathrm{Re}\nu_\ell$ and damping directly proportional to $\mathrm{Im}\nu_\ell$. In this case, the pulse envelope change must be attributed not to dispersion but to differential attenuation of the wave components which are all generated simultaneously

at the tangent and whose superposition comprises the net creeping wave. Actually, according to the theory, the different frequency components of which the pulse is composed are known to propagate on the boundary with different velocities. Not only that, but the components even at a single frequency or ka, travel at different velocities. However, to within experimental resolution, both of these effects are not observable since in Fig. 5 the individual cycles of the pulse occur at the same relative times. Thus the measurement of a velocity by a differential-path method results in a unique determination which may be called the wave velocity. Differences between phase, group, or signal velocity, are below the limits of accuracy of these measurements; they are not measurable in the cases reported here.

The velocity and attenuation were determined by a series of measurements demonstrated in Fig. 3. The receiving hydrophone was rotated about the diffracting-cylinder axis in 10° increments in successive measurements. The ratio of the difference in path along the cylinder surface to the time difference in pulse arrival at the hydrophone is an expression of the desired circumferential velocity. A multiple exposure of the pulses received at position two through six in Fig. 3 is shown in Fig. 6 and shows the attenuation of the pulse.

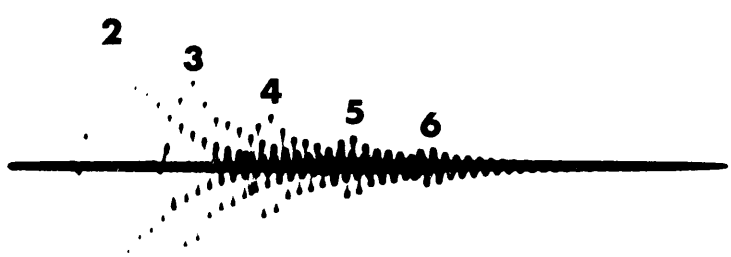

Fig. 6—Multiple exposure of the acoustic pulse received at positions 2 – 6 in Fig. 3.

This Franz wave is primarily related to the geometric form of the diffracting object but is also significantly affected by the composition of the body. The latter fact was verified by experimental measurement of the circumferential speed (c_c) and attenuation of the Franz wave on an aluminum (type 6061) cylinder. In the plot of Fig. 7, the experimental values of c_c/c_w given in Table II are plotted versus the size parameter (ka). Values of the wave speed ratio computed by the formula of Franz for rigid cylinders valid

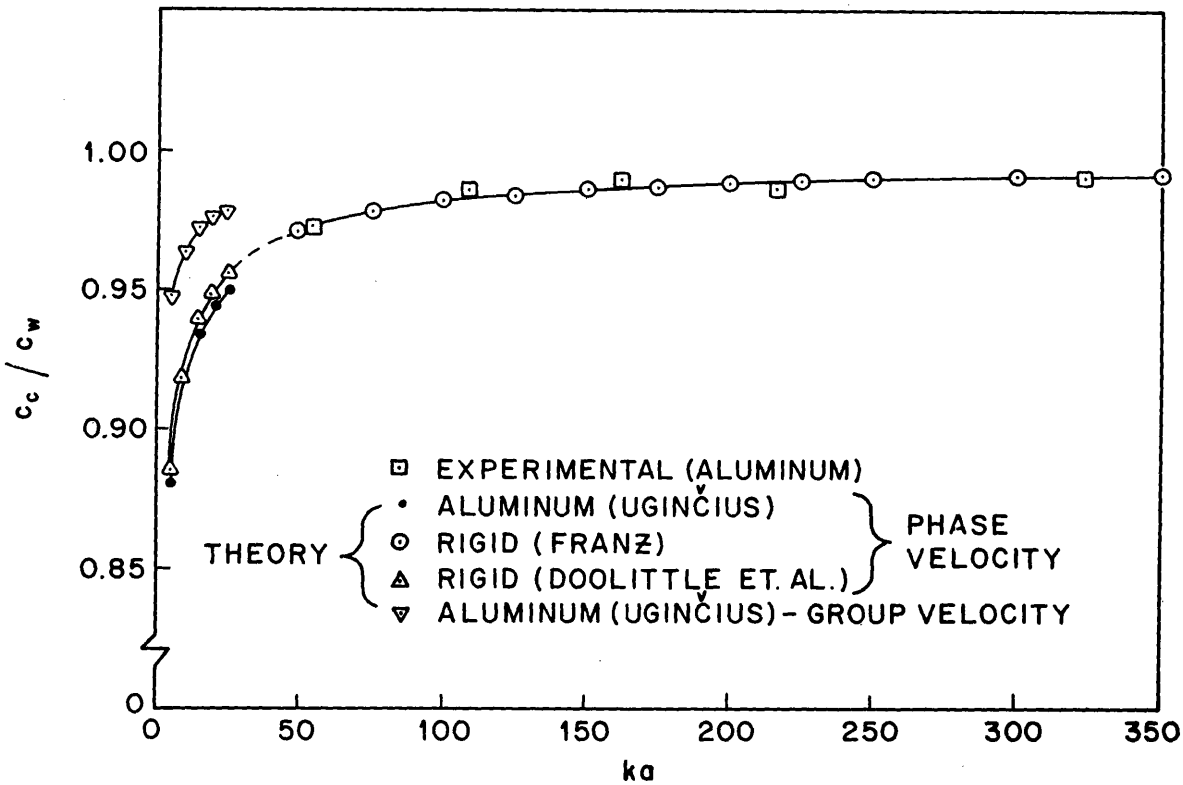

Fig. 7—The comparison of experimental measurements and various theoretical calculation of the Franz-wave velocity as a function of size parameter (ka).

TABLE II

VELOCITIES AND ATTENUATIONS OF THE "FRANZ TYPE" WAVE FOR ALUMINUM CYLINDERS OF VARIOUS SIZES.

Size Parameter ka	Diameter (cm)	Attenuation (Np/rad)		Velocity (c_c/c_w)	
		Experiment	Theory	Experiment	Theory
54.0	2.54	1.97	2.68	0.973	0.973
107.9	5.08	2.17	3.36	0.985	0.983
161.9	7.62	2.50	3.84	0.989	0.987
215.8	10.16	2.77	4.22	0.987	0.989
323.7	15.24	2.98	4.83	0.990	0.992

for large ka (Eq. 1) are also plotted. The line connecting these values reasonably should and in fact does connect up smoothly with the calculations for the rigid solid cylinder given by Doolittle, et al. The computation of both phase and group velocity for an essentially solid aluminum cylinder at ka below 25 according to Uginčius are also plotted. At the values of ka measured, the velocity of the Franz wave agrees with theory, according to Eq. 1, to within experimental error of the measurements, which was ±0.5%. This accuracy is represented by the vertical dimension of the squares surrounding the experimental points. It is interesting to notice that the curve for an aluminum cylinder at low ka seems reasonably to approach the curve for the rigid case at high ka. According to experimental results, this will occur at a value of ka as low as 54. These data plotted in this way also show consistency with the conclusion that phase velocity is the quantity being measured.

Experimental values of attenuation of the Franz wave for an aluminum cylinder were measured and are also found in Table II. In Fig. 8, these data are plotted in units of

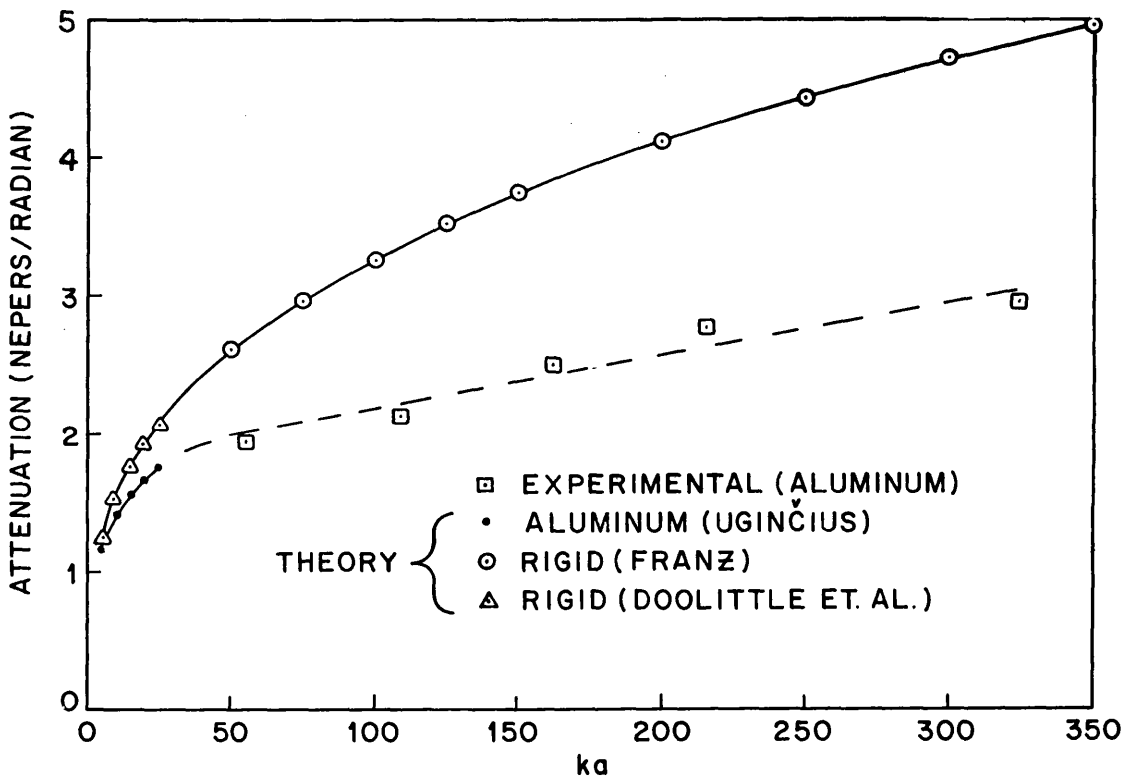

Fig. 8– The comparison of experimental measurements and theoretical calculations of Franz-wave attenuation as a function of size parameter (ka).

Np/rad versus ka. Again the values calculated by Franz's formula (Eq. 1) are plotted at high ka and connected to those of Doolittle, et al., for low ka. The curve for the aluminum cylinder, again according to Uginčius, shows a marked difference from the rigid case even at a ka of 25. The least square fit to the experimental points at high ka is in reasonable agreement with an extension of the points of Uginčius at low ka, showing a drastic difference with the curve for the rigid case. This difference is caused by the elasticity of the cylinder. These results are the first observation and specific identification of this type of wave for pulsed signals in water.

The Franz wave was also measured for aluminum shells. It was found at high ka (215.8) that a thin shell with inside to outside diameter ratio (b/a) of up to 0.99 acts like a rigid cylinder. The experimental data are given in Table III. This indicates quite

TABLE III

EXPERIMENTALLY MEASURED VELOCITIES AND ATTENUATIONS OF THE "FRANZ TYPE" WAVE FOR ALUMINUM CYLINDRICAL SHELLS OF VARIOUS WALL THICKNESSES FOR ka = 215.8 (diameter = 10.16 cm)

b/a	Wall Thickness (cm)	Attenuation (Np/rad)	Velocity (c_c/c_w)
0.00	--	2.77	0.986
0.60	4.06	2.74	0.986
0.70	3.05	2.76	0.984
0.80	2.03	2.70	0.986
0.90	1.02	2.78	0.990
0.99	0.03	2.64	0.989

reasonably that the degree to which a shell acts as a hard or soft cylinder is a function of whether the cylinder wall thickness is large or small respectively relative to the wavelength of the incident sound. Uginčius found that at low ka (ka = 5) an aluminum shell behaves like a rigid scatterer for $b/a \lesssim 0.75$. Experiment shows that at ka = 215.8 even for $b/a \leq 0.99$ the shell acts rigid. Practical limitation of making the thin shell prevented measurements at higher b/a.

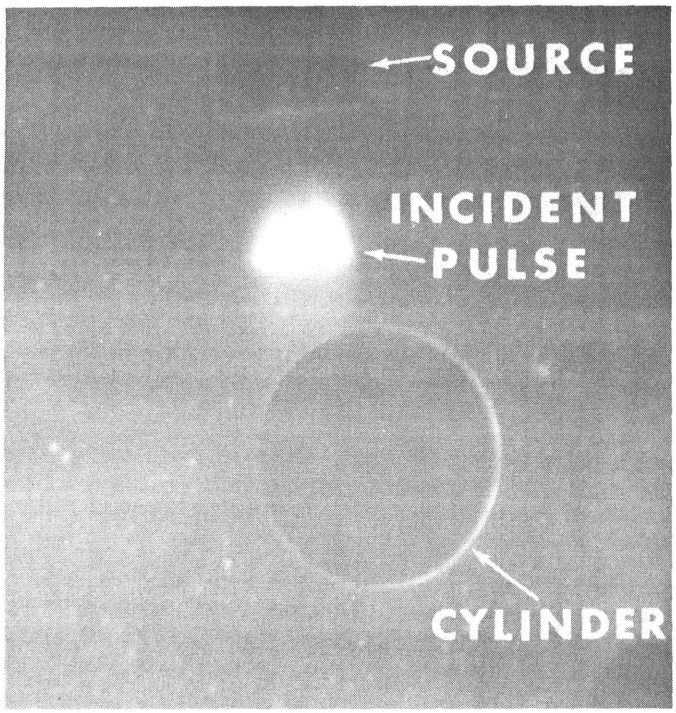

Fig. 9– Schlieren photograph of an acoustic pulse prior to falling incident on an aluminum cylinder in water.

surrounding medium is water. All Schlieren pictures were taken with a 5-MHz-acoustic source. The transducer is seen at the top of the figure and the pulse of approximately 5-μsec duration which is emitted by the source is shown before it strikes the curved surface of the cylinder which is seen in the figure in cross section as the dark disc. The brightened outline of the disc is caused by very slight imperfection in the alignment of the cylinder along the parallel beam of the Schlieren system accentuated by the highly polished curved surface of the cylinder. In Fig. 10, the center of the acoustic beam is incident at the tangent point at the left extreme of the cylinder. The curved wavefront

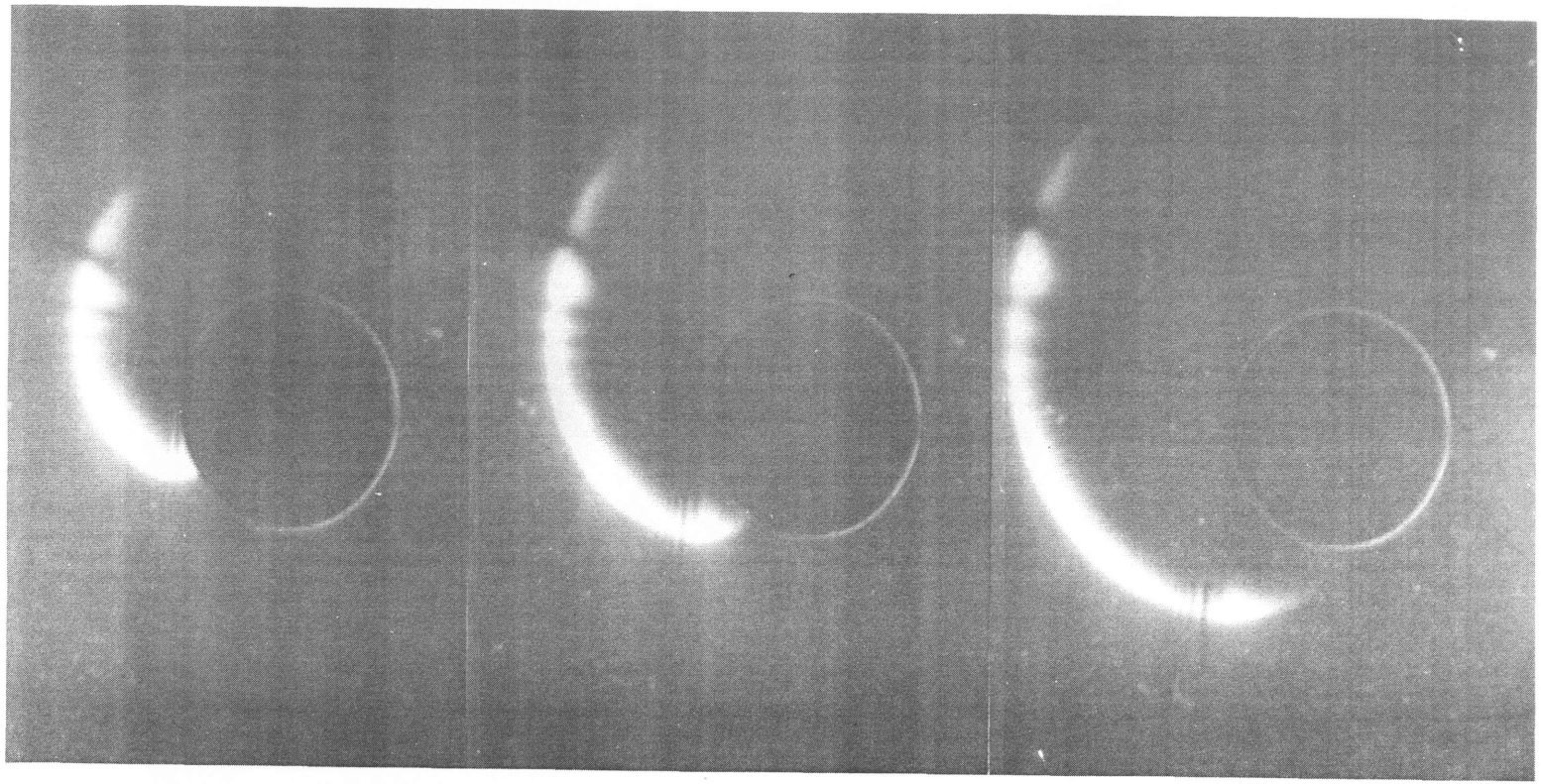

Fig. 10—Schlieren photographs of the Franz wave at three successive times for an aluminum cylinder in water (ka = 323.7).

to the left of a vertical line tangent to the cylinder is the specular reflection from the cylinder's curved surface. In Fig. 10(a), the "Franz wave" is seen soon after launching and 10(b) and (c) show the wave at successfully later times. The wave is so rapidly attenuated that its extension to the cylinder in Fig. 10(c) is not visible. A clearer picture of the wave can be seen in Fig. 11(a) and (b). In this case, the "Franz wave"

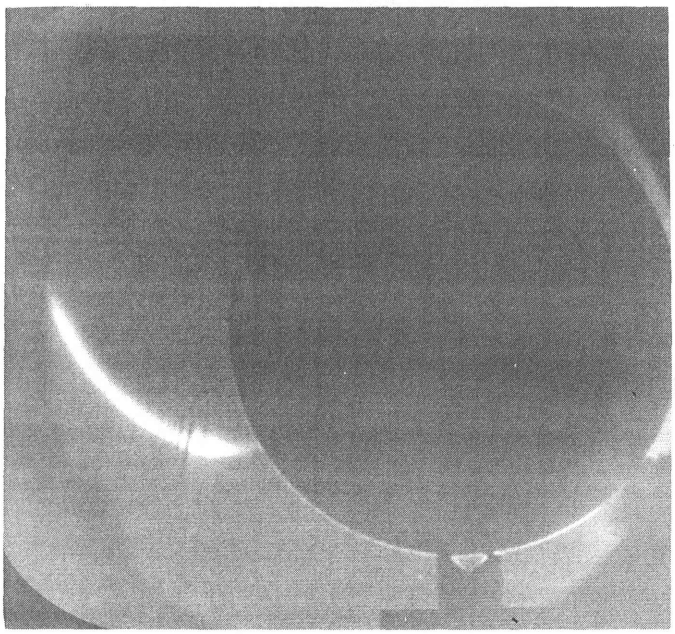

Fig. 11(a)—Schlieren photograph of the wavefront resulting from the Franz wave for an aluminum cylinder in water (ka = 1008).

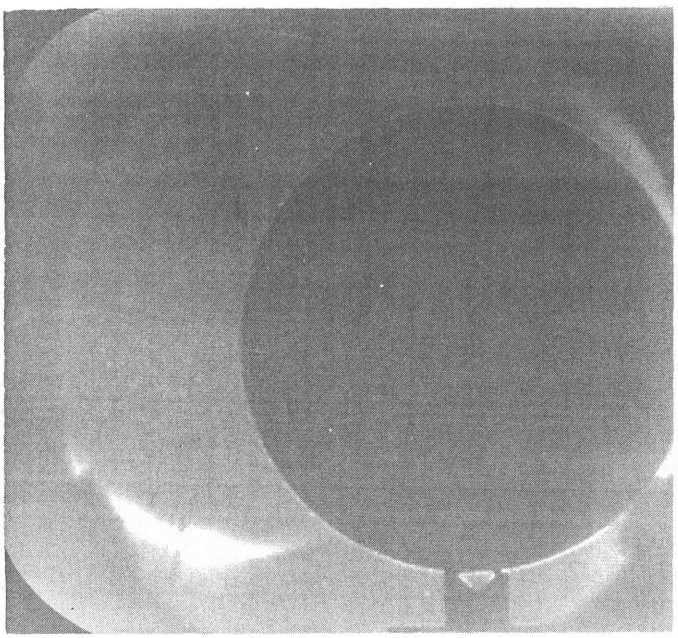

Fig. 11(b)—Schlieren photograph of the wavefront resulting from the Franz wave for an aluminum cylinder in water at a later time than in Fig. 11(a).

is seen to the right of the striations in the wavefront. The striations deserve a few words of explanation and are probably significant enough to warrent further study. Their major cause is certainly the interference between the direct wave from the transducer and the specular reflection from the curved cylinder surface near the point of tangent incidence. However, calculations of the interference spacing along the wavefront using only these two waves do not correspond as closely as one would expect to the measurements taken from the photographs. Discrepancies between measured inter-null spacings and those which were calculated were as large as 50%. Undoubtedly a significant contribution to the interference pattern is the portion of the incident beam to one side of the central axis of the source, which falls on the cylinder very near grazing incidence. To examine this effect further, refinements in both the acoustic and Schlieren systems would be required to accentuate important features. Schlieren photographs of a cylinder at a ka of 215.8 are shown in Fig. 12. It is interesting to notice that there is no evidence in any of these photographs of a wave returning in the direction of the source which originated at the so called boundary of the shadow region as formulated by the "image pulse concept" of Freedman[24]. With the data taken from Fig. 11(a) and (b), a geometric construction was made of the wavefront. This is shown in Fig. 13. A construction similar to Fig. 13 is given by Friedlander[25].

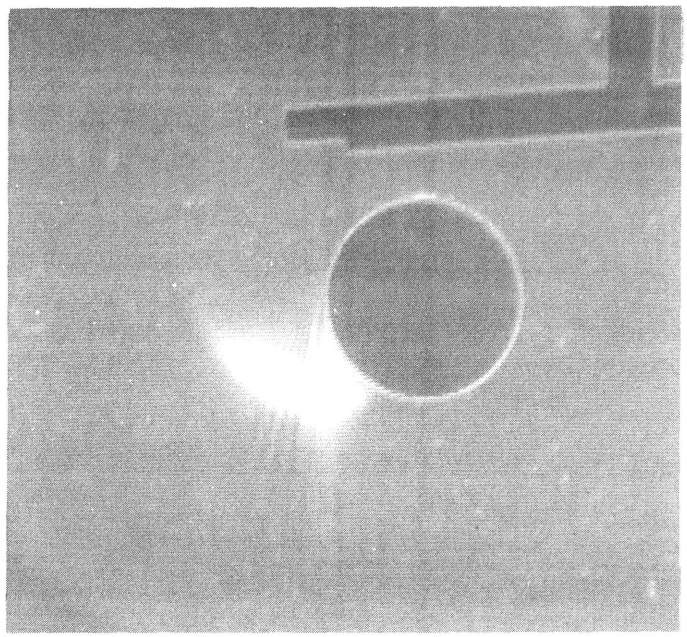

Fig. 12(a)–Schlieren photograph of the wavefront resulting from the Franz wave for an aluminum cylinder in water (ka = 215.8).

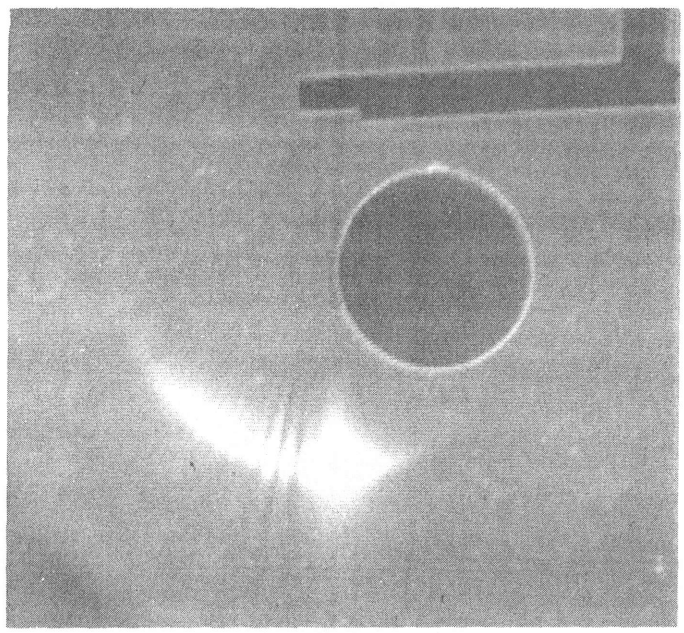

Fig. 12(b)–Schlieren photograph of the wavefront resulting from the Franz wave for an aluminum cylinder in water at a later time than in Fig. 12(b).

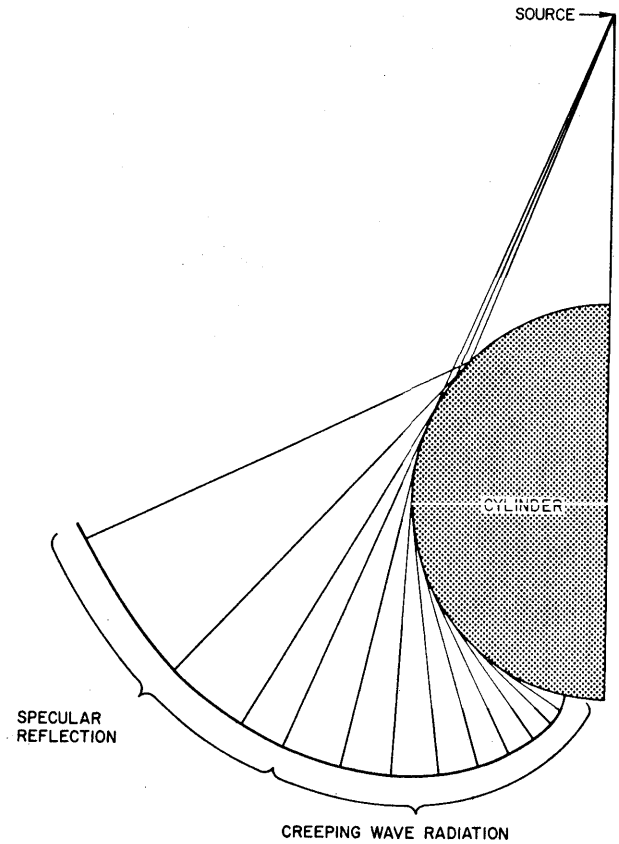

Fig. 13—Geometric construction reproducing the features of the wavefront caused by the generation of the Franz wave.

II – The "Rayleigh Type" Wave

The same experimental configuration which was used to investigate the "Franz type" wave was used to generate a second type of wave which travels circumferentially within the surface of the cylinder. This time, however, the central axis of the source beam was directed at an incidence angle of approximately 30° at the cylinder surface. Figure 14 shows schematically, the propagation path of the wave which occurred when the source beam was so directed. The wave once generated, is propagated along the inside of the curved boundary of the cylinder's surface. The spiral on the outside of the cylinder is merely illustrative; the path inside the boundary is actually identical on successive

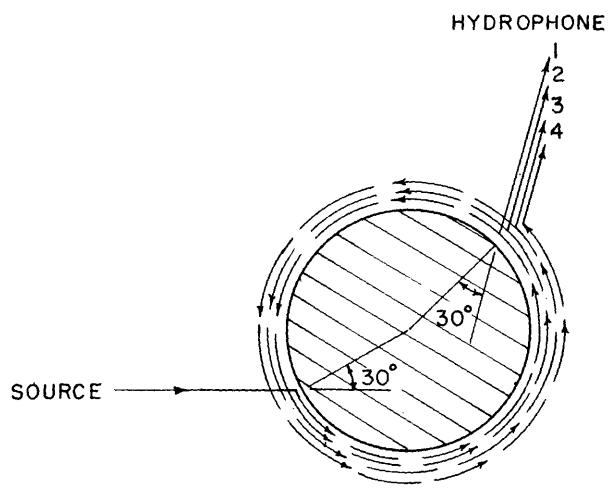

Fig. 14–Experimental configuration for observing and measuring the properties of the refracted circumferential wave generated at 30° incidence. The spiral path represents a wave which travels on the inside of the boundary over an identical path on successive circuits. The paths to and at the points labeled 1 – 4 are to be considered coincident at the hydrophone.

circuits around the cylinder. As the wave propagates along the circumference, it constantly radiates energy out into the field in the water surrounding the cylinder at an angle of 30°. A hydrophone placed as indicated in Fig. 14 would receive that wave propagated along a line making the same emergence angle as the incidence angle. Since only part of the wave's energy is radiated off at any one position, energy remains in the circumferential wave which ultimately circumnavigates the cylinder any number of times, producing a pulse at the hydrophone on each circuit. The pulse sequence received by a hydrophone whose location is indicated in Fig. 14 and seen in Fig. 15. In this case,

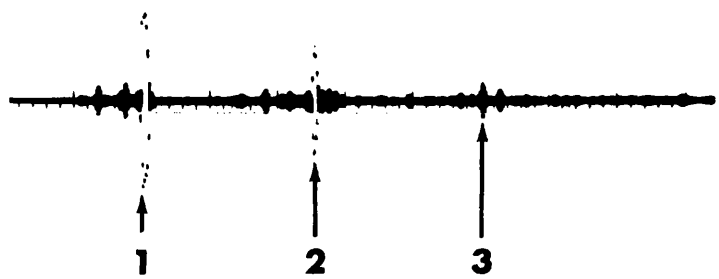

Fig. 15—The pulse sequence detected by 2.54-cm-disc hydrophone placed as shown in Fig. 14 for a cylinder of ka = 323.7. The time between labeled pulses is 129 μsec.

the cylinder had a diameter of 15.24 cm (6 in.) having a ka of 323.7. The labels 1 through 4 correspond to the time sequence of pulse reception indicated in Fig. 14. The time between the labeled pulses is 129 μsec. It can be seen in all of the pulse sequences that a background of pulses exists other than those which are labeled. This indicates that at incidence angles on the cylinder which occur within the same beam, other waves are produced which may be traveling through the cylinder or which may be other circumferential waves. It is not sufficient to identify a sequence of pulses which have a fixed time interval to identify circumferential waves, since it is possible to adjust transducers to obtain an erroneous result or at least an inconclusive one. To avoid erroneous results, unique wave identification is accomplished by rotating the hydrophone (at a constant distance) about the cylinder axis so that the pulses can continue to be identified but retain a fixed interpulse spacing. Further it was possible to rotate the hydrophone through a sufficient angular distance so that a differential-path measurement of wave

speed was also made. When the wave was properly identified, the same wave speed resulted. For ka=323.7, c_c/c_w was 2.54, i.e., the circumferential wave speed (c_c) was 2.54 times the free-wave speed (c_w) in water. The acoustic source for these measurements was the same 2.54 cm-square source used in the "Franz type"-wave measurements. The hydrophone was a 2.54-cm diameter-lead-zirconate-titanate disc resonant at one MHz. The large hydrophone was used to obtain an increased electrical output which will be an accurate representation of the wave only if the signal on its entire face is of constant phase or in other words the incident wave is plane or essentially so, since the electrical output is the integral of the pressure over the area of the hydrophone. A true representation of a wave at a point in its path will be detected by a probe or a small hydrophone.

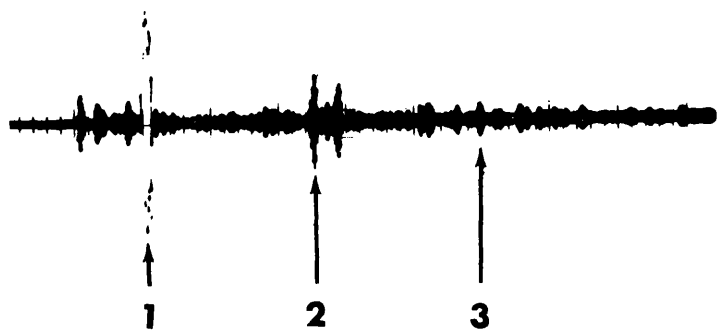

Fig. 16—The same insonfication of the same cylinder (ka = 323.7) as used to obtain Fig. 15 except with a small more omnidirectional hydrophone closer to the cylinder surface. The time between labeled pulses is 129 μsec.

The same pulse sequence shown in Fig. 16, was detected with a hydrophone with a sensing disc 0.160 cm diam and the identical cylinder insonification which was used to obtain Fig. 16 with a 2.54-cm-diam disc. The small hydrophone was moved closer to the cylinder surface since its sensitivity was lower than the larger hydrophone. It can be noticed that the background of extraneous pulses is different in the two cases but the labeled pulses are also 129 μsec apart. Pulse sequences from which circumferential velocities and attenuations for ka of 215.8 and 161.9 were obtained are shown in Figs. 17 and 18 respectively. These data are given in Table IV. It is significant that the values

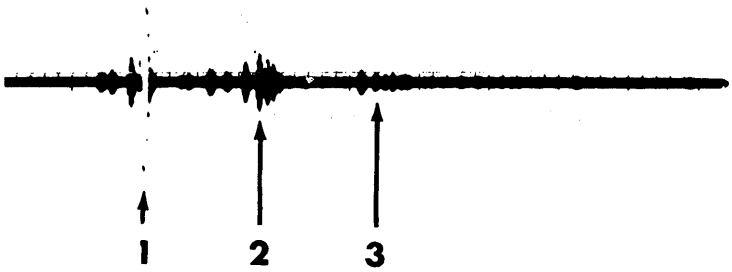

Fig. 17—The pulse sequence detected by a hydrophone placed as shown in Fig. 14 for a cylinder of ka = 215.8.

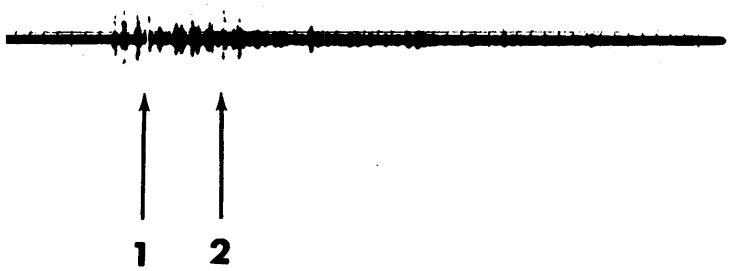

Fig. 18—The pulse sequence detected by a hydrophone placed as shown in Fig. 14 for a cylinder of ka = 161.9.

TABLE IV

EXPERIMENTALLY MEASURED VELOCITIES AND ATTENUATION OF THE REFRACTED CIRCUMFERENTIAL WAVE GENERATED AT 30° INCIDENCE ON ALUMINUM CYLINDERS OF VARIOUS SIZES.

Diameter (cm)	Size Parameter ka	Velocity c_c/c_w	Attenuation (Np/rad)
5.08	107.9	2.98	–
7.62	161.9	2.86	–
10.16	215.8	2.52	0.17
15.24	323.7	2.52	0.10

for velocity increase with decreasing ka which shows qualitative consistency with the motion of the appropriate pole (R1) in the calculations of Uginčius, although quantitative agreement is not found. Also, although there are but two measurements of attenuation, this quantity also varies in a manner similar to that predicted by Uginčius. The lack of quantitative agreement with theory and the absence of some experimental values for attenuation will be discussed in Chapter V. It may be observed in Fig. 18, that as ka becomes smaller, the successive circuits of a circumferential pulse become harder and

harder to identify. This is true because the beam width of the source is constant at its resonant frequency and it illuminates a larger portion of the cylinder as the cylinder becomes small, permitting the exitation of more types of waves.

Schlieren photographs of the isolated wave generated at approximately 30° incidence are shown at two different times in Figs. 19(a) and (b) for ka of 323.7. The bright region at the face of the source is caused by heat radiation from a heat buildup in the lens covering the vibrating disc. This focused transducer was used to restrict the region of

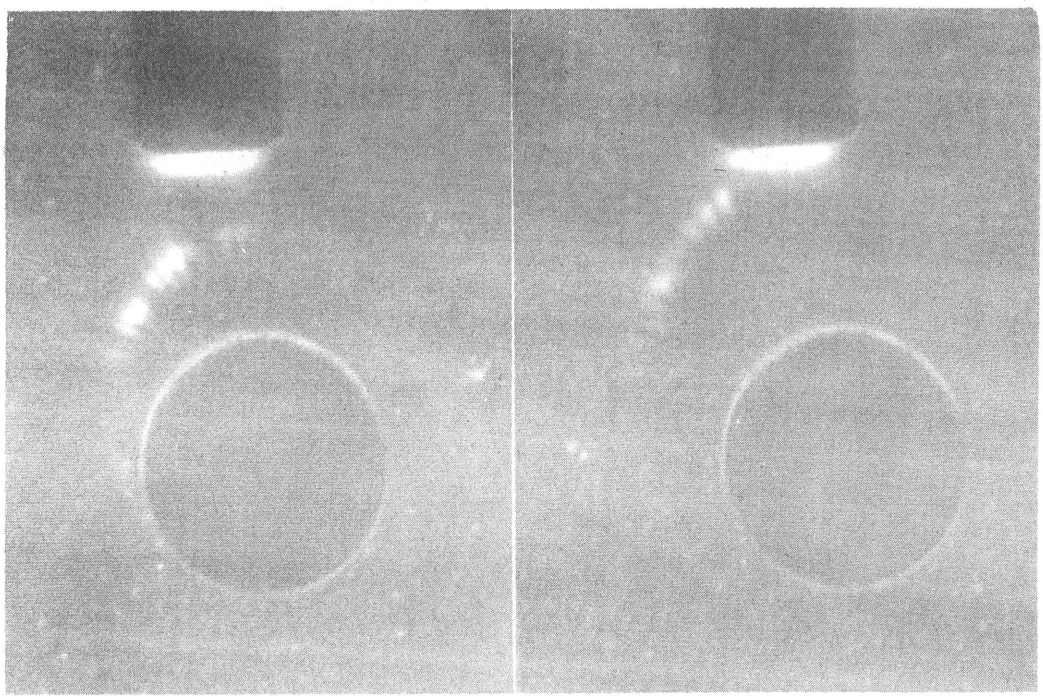

Fig. 19(a)—Schlieren photograph of the radiated wavefront resulting from the circumferential wave generated at a 30° incidence angle (ka = 323.7).

(b)—Same as Fig. 19(a) except at a later time.

insonification in order to generate only the one isolated wave. However, the converging rays resulting from the focused transducer did not seem to generate the waves sufficiently to get a bright picture.

A diagram intended to clarify and aid in the interpretation of the Schlieren photographs of the internal circumferential waves is given in Fig. 20. The incident "ray" generates the usual specular reflection at the cylinder surface. Also at the surface the circumferential wave is generated and propagated along the boundary, diminishing in amplitude as it progresses as indicated by the arrow head sizes. Radiation occurs into the medium surrounding the cylinder at the same angle (θ) as the incident angle. A wave front is generated which propagates in the direction of the "rays" issuing from the cylinder surface. At some time $t = t_1$, it has the position shown on the inside of the solid line showing its position at $t = t_2$. The wavefront radiated as a result of the circumferential wave does

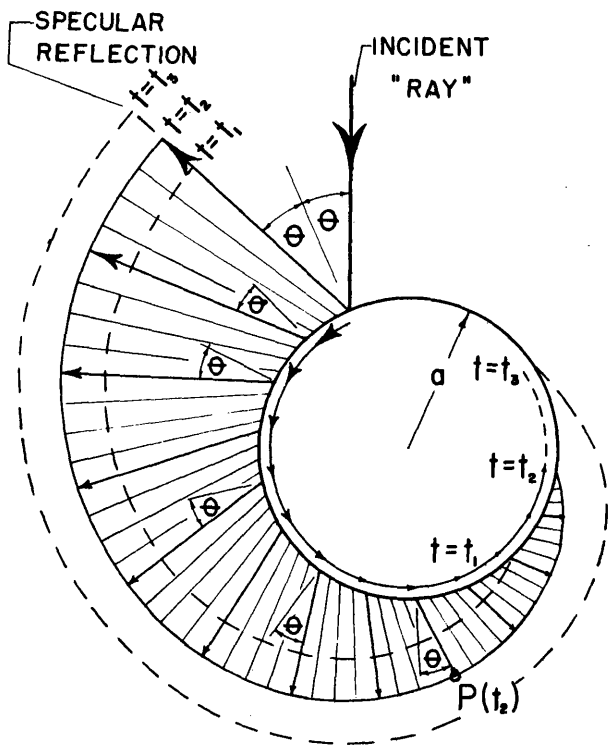

Fig. 20—General geometric construction for the refracted circumferential wave showing time progression and the relationship between the wavefront and hydrophone data.

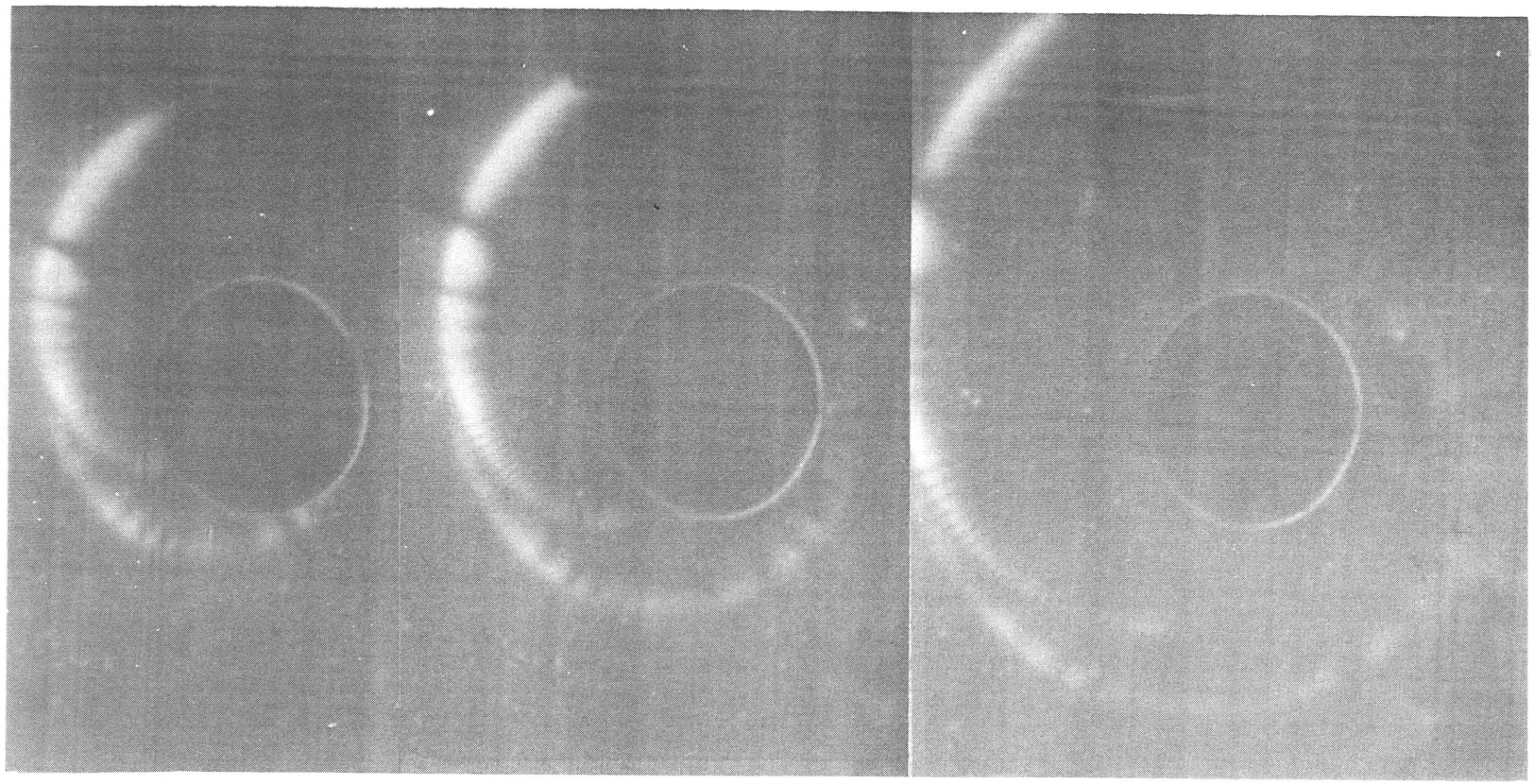

Fig. 21—Schlieren photograph of the wavefront resulting from the simultaneous generation of Franz wave and the circumferential wave generated at 30° incidence at three successive times for an aluminum cylinder in water (ka =323.7).

not have a constant amplitude along its length as indicated by the arrow head sizes for the wavefront at $t = t_2$. The same cylinder used to obtain Fig. 19 was insonified with a non-focused transducer at the same time both in the region of the tangent and in the region of 30°. Thus the Franz wave was generated in addition to the wave at 30°. The Franz wave is seen behind the faster refracted circumferential wave. Three successive times in the propagation of the waves are shown in Figs. 21(a), (b), and (c).

The same type wave was generated for a cylinder with a ka of 1008, where its isolation is simpler since the source beam width covers a smaller angular area on the cylinder surface. The result is shown in Fig. 22(a) and (b) at two successive times. In this case, the wavefront is significantly narrower consistent with the smaller initial illuminated area and showing that the surface-wave-generated front is smoothly continuous with the specularly-reflected-pulse front. This is a significant observation since it shows that the internal wave in the cylinder is indeed a boundary or surface wave since if it were not, the internal wave would have to travel with a speed approaching ∞ within the cylinder in order to produce a smooth continuous front with the totally external specularly reflected wave. This reasoning can be applied to the "rays" of the diagram in Fig. 20. Confirmation of the continuity of the isolated specular reflection with the surface generated radiated wavefront can be seen in Fig. 23(a), (b), and (c) for ka = 215.8.

Schlieren visualization of waves is a valuable adjunct to the quantitative pressure field measurements taken with a hydrophone. It is extremely difficult to obtain precise quantitative data from the Schlieren photographs. It was, however, possible to establish the fact that the Schlieren photographs are consistent with the hydrophone measurements by the following method. The central axis of the beam emitted by the source was drawn from the source center normal to its surface to the point where it intersected the cylinder. From that point, the specular direction was determined by estimating the center of the specularly reflected pulse. The ratio of the circumferential wave speed to the free-wave speed in water was determined from the Schlieren photographs by taking the ratio of the length of the path in the specular direction to the length of the path along the circumference at the point where the radiated wavefront intersected the cylinder surface. The

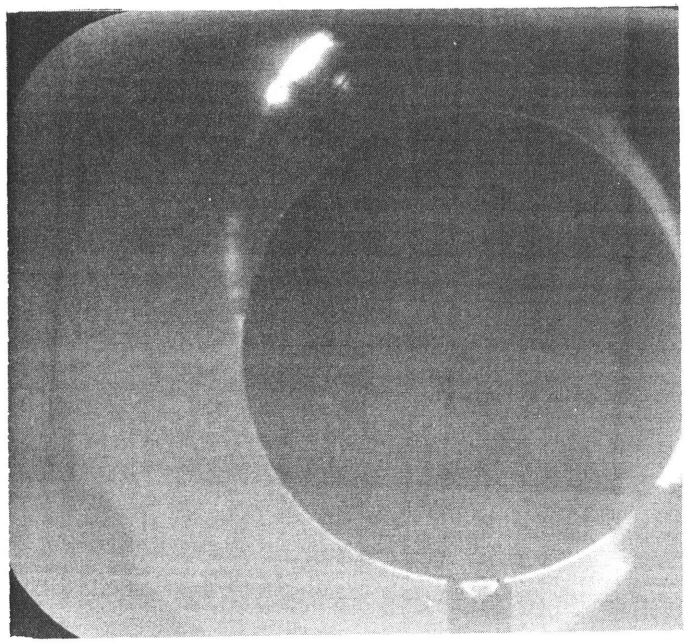

Fig. 22(a)—Schlieren photograph of the wavefront resulting from the circumferential wave generated at 30° incidence for an aluminum cylinder in water (ka = 1008).

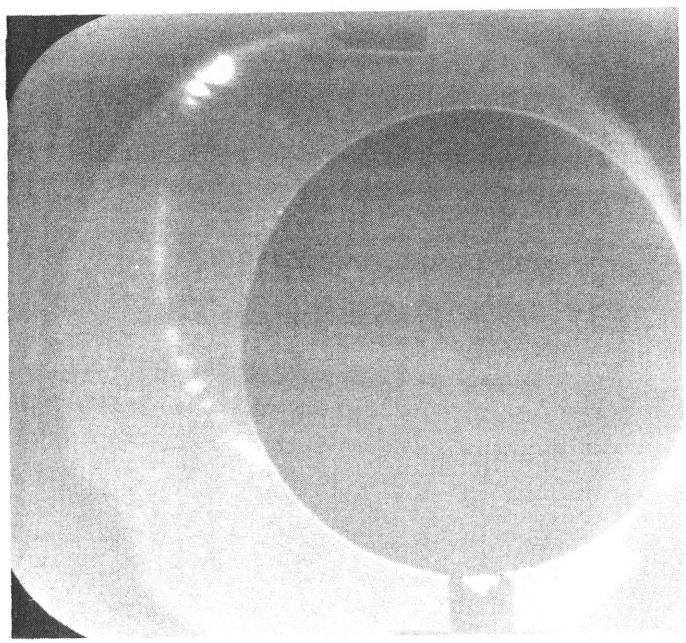

Fig. 22(b)—Schlieren photograph of the wavefront resulting from the circumferential wave generated at 30° incidence at a later time than in Fig. 22(a).

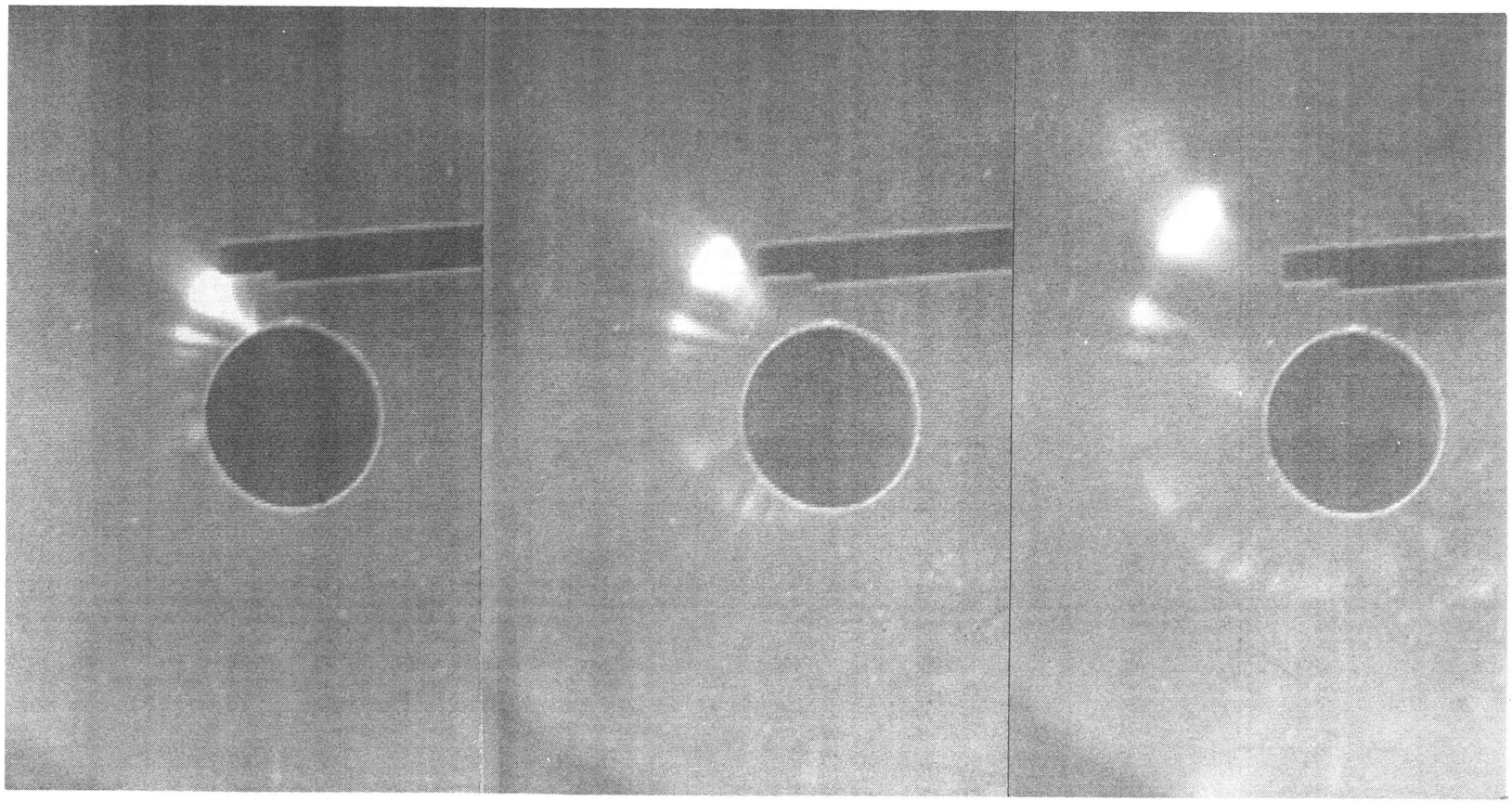

Fig. 23—Schlieren photographs of the wavefront resulting from the circumferential wave generated at 30° incidence at three successive times for an aluminum cylinder in water (ka = 215.8).

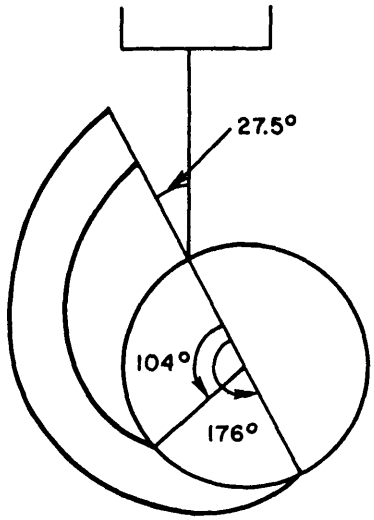

Fig. 24– Geometric construction corresponding to the Schlieren visualization of wavefronts of Figs. 19(a) and (b) at ka = 323.7.

entire wavefront can be reconstructed as shown in Fig. 24 by using this ratio to establish points on the wavefront between the specular pulse and the point where the circumferential wave is just beginning to radiate from the cylinder. The path from the point of wave incidence to any point on the wavefront must satisfy certain conditions. The total wave path from the point of incidence to all points on the wave front must equal the specular wave path. Also, the emergence angle at the cylinder surface must be in all cases equal to the incidence angle. Now all paths and speeds are determined and the construction of the wavefront should be consistent with the physical measurement of the presumed properties if the waves are correct. The wave-speed ratio c_c/c_w averaged for two times in Fig. 24 is 2.4 which is in reasonable agreement with the hydrophone data result of 2.5 for a ka of 323.7. The wave generated at 30° incidence was also measured on shells ranging in inside-to-outside-diameter ratio (b/a) of zero to 0.99 at a ka of 215.8. The data (Table V) shows no significant changes in circumferential wave attenuation for the cases measured, but indicate a variation in velocity similar to that calculated by Uginčius for such a case at a ka of 5. Unfortunately, the lack of accuracy in the measurement of attenuation prevented significant plotting of pole locus for this ka. Figure 25 is a wavefront construction similar to Fig. 24 for a ka of 215.8 (Fig. 23). At this ka, the geometric construction resulted in a value of c_c/c_w of 2.5 which is the same as the hydrophone result.

A discussion and theoretical derivation of the complex critical angle at which a refracted circumferential wave is generated is given in Ref. 12. A practical approximation

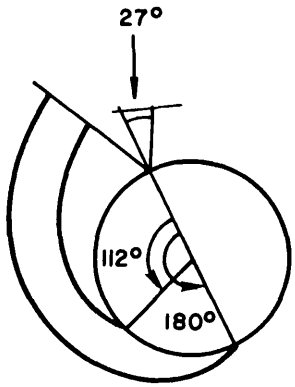

Fig. 25–A geometric construction corresponding to the first two parts of Fig. 23 (ka = 215.8).

TABLE V

VELOCITIES AND ATTENUATIONS OF THE "RAYLEIGH TYPE" WAVE FOR ALUMINUM CYLINDRICAL SHELLS OF VARIOUS WALL THICKNESSES FOR ka = 215.8 (DIAMETER = 10.16 cm).

b/a	Wall Thickness (cm)	Attenuation (Np/rad)	Velocity (c_c/c_w)
0.00	–	0.272	2.52
0.60	4.06	0.318	2.25
0.70	3.05	0.299	2.21
0.80	2.03	0.266	2.43
0.90	1.02	0.288	2.14

to the theoretically predicted value may be considered to be expressed as

$$\theta \approx \sin^{-1} (c_w/c_c). \tag{5}$$

Substituting the experimentally measured values of c_w and c_c in Eq. 5, the angle (θ) at which a circumferential wave should be generated is 23° for a ka of 323.7. Considering the approximations of the theory and the inaccuracy of the incidence-angle measurement in the experiment, the theoretical value compares favorably with the nominal 30° measurement for this wave.

III – A Third Circumferential Wave.

With the identical apparatus used to measure the properties of and observe the resultant radiated wave of both the Franz-type wave and the wave generated at a 30° incidence angle, a third circumferential wave was observed which was characteristically generated at approximately 15° incidence and emergence angle for aluminum cylinders immersed in water. The schematic diagram in Fig. 26 represents the identical successive circumferential paths as a spiral on the outside of the cylinder for illustrative purposes as was done

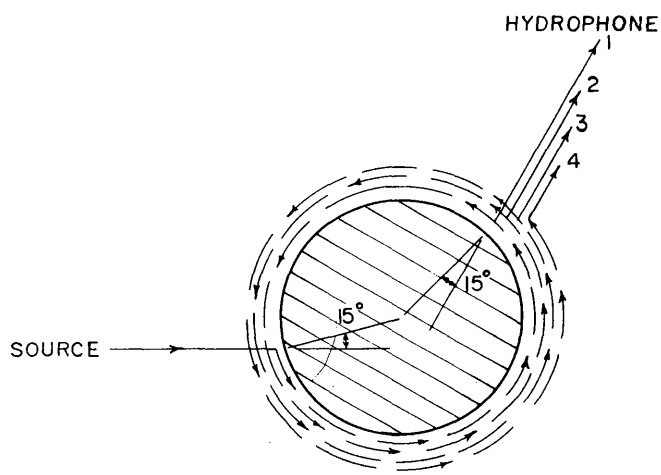

Fig. 26–Experimental configuration for observing and measuring the properties of the refracted circumferential wave generated at 15° incidence. The spiral path represents a wave which travels on the inside of the boundary over an identical path on successive circuits. The paths to and/at the points labeled 1 – 4 are to be considered coincident at the hydrophone.

in Fig. 14 for the wave generated at a 30° incidence angle. Again in this case the wave path is on the inside of the boundary. The sequence of pulses received at a hydrophone placed at the fixed position, shown in Fig. 26, is shown in Fig. 27. The pulse spacing

Fig. 27—The pulse sequence detected by a hydrophone placed as as shown in Fig. 26 for a cylinder of ka = 323.7. The time between labeled pulses is 49 μsec.

is 29 μsec which corresponds to the radiation from successive circuits around the circumference of a cylinder with a diameter of 15.24 cm (6 in.). This corresponds to a speed of this wave of 6.5 times the speed of a free wave in water. The same qualitative physical interpretation applies to these results as given in Figs. 15–18. The experimental data for the 15° incidence wave are given in Table VI. The conclusions from these data

TABLE VI

EXPERIMENTALLY MEASURED VELOCITIES AND ATTENUATION OF THE REFRACTED CIRCUMFERENTIAL WAVE GENERATED AT 15° INCIDENCE ON ALUMINUM CYLINDERS OF VARIOUS SIZES.

Diameter (cm)	Size Parameter ka	Velocity c_c/c_w	Attenuation (Np/rad)
5.08	107.9	7.44	–
7.62	161.9	6.78	0.14
10.16	215.8	6.57	0.10
15.24	323.7	6.64	0.08

are the same about this wave as those concluded from the 30° incidence-wave data in Table IV, making it reasonable to conclude that this is a higher order, i.e., Rn, pole-related wave.

Data on shells of various thicknesses at a ka of 215.8, similar to those in Table V, for this wave were sought but so many waves were present for such shells at shallow angles that unique values and wave identification was impossible. Figure 27 represents results for ka = 323.7. The same result is shown in Fig. 28 except with the hydrophone

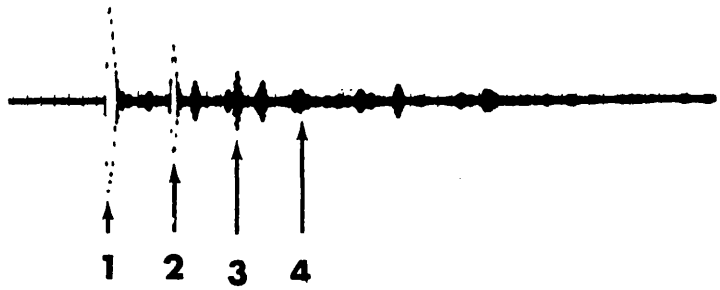

Fig. 28—The same conditions as in Fig. 27 except with the hydrophone rotated about the cylinder axis, clockwise to a different position. The time between labeled pulses is 49 μsec.

rotated about the axis of the cylinder (clockwise) to a position so that the initial path from source to hydrophone is shorter as evidenced by the occurrence of the first pulse at an earlier time on the independently-triggered-oscilloscope trace. Two interesting observations can be made in comparing Figs. 27 and 28 in addition to the fact that they can be and were used to measure the wave speed by a differential path method. At different positions of the hydrophone, a different background sequence of (so called) extraneous pulses is present and the amplitudes of the background pulses seem to be fairly constant and are somewhat higher relative to the data pulses than in the case of the wave generated at a 30° incidence angle. This indicates that this faster refracted wave is generated to a lesser degree than the slower refracted wave. Pulse sequences for the same values of ka as were given for the 30° incidence case shown in Fig. 29 for ka = 215.8 and in Fig. 30 for ka = 161.9. Corresponding velocity and attenuation data are given in Table VI. It is obvious from the relative magnitude of pulses having made successively more circuits, that this wave is less attenuated than the slower wave which is generated at 30° incidence.

Visualization by the Schlieren method of the wavefront radiated by this circumferential wave was carried out for all of the same values of ka as for the wave at 30°

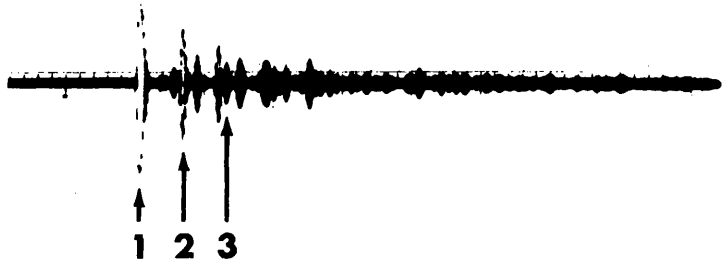

Fig. 29—The pulse sequence detected by a hydrophone placed as shown in Fig. 26 for a cylinder of ka = 215.8.

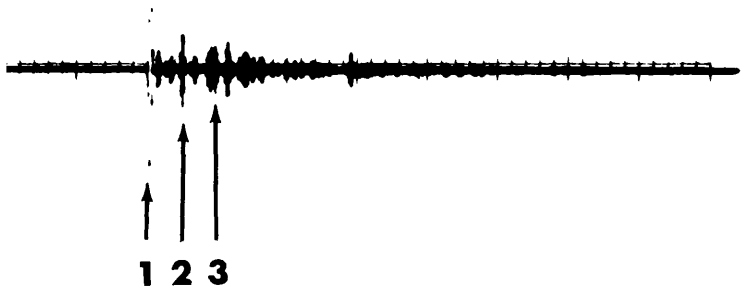

Fig. 30—The pulse sequence detected by a hydrophone placed as shown in Fig. 26 for a cylinder of ka = 161.9.

incidence. For the case of ka = 323.7, shown in Fig. 31(a) and (b) at two different times, it can be seen that since the circumferential wave has such a high speed relative to the free water-borne-wave speed, the radiated wavefront resulting from the circumferential

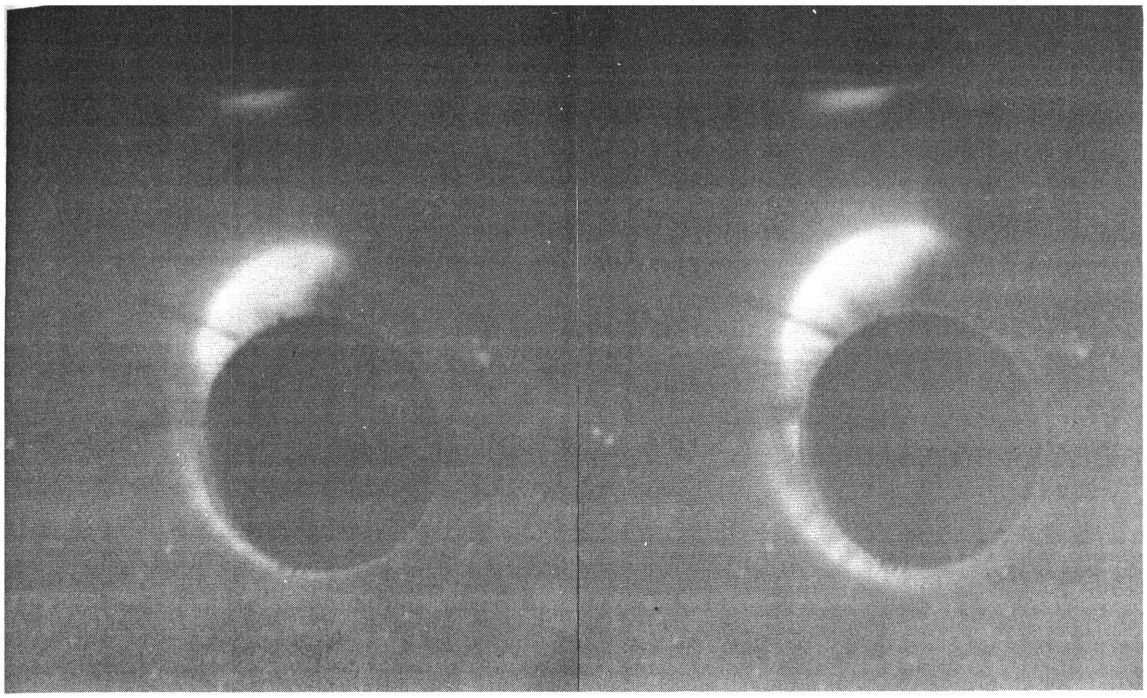

Fig. 31(a)–Schlieren photograph of the radiated wavefront resulting from the circumferential wave generated at a 15 deg incidence angle (ka = 323.7).

(b)–Same as Fig. 31(a) except at a later time.

wave has a curvature very nearly that of the curved cylinder surface itself. This makes it very difficult to determine the point at which the wavefront touches the cylinder even though this circumferential wave has relatively little attenuation. Also, as indicated by the brightness of the wavefront resulting from the circumferential wave, relative to the brightness of the specular reflection this faster wave is generated to a less degree than the slower refracted circumferential wave. This was also concluded from the hydrophone data. For the parameters chosen to get ka of 323.7 at 5 MHz, the unfortunate circumstance occurred that the direct through-compressional wave through the body of the cylinder emerged very close to the same time as the radiated-circumferential wave in the neighborhood of 150° – 180°. This caused a broadening of the wavefront which is obvious in Fig. 31(b). It is for the same reasons as stated before that at the higher ka of 1008 in Fig. 32(a) and (b), a sharper definition of the wavefront is achieved. Schlieren photographs of two times for a ka of 215 are given in Fig. 33(a) and (b).

A wavefront construction similar to that described in Fig. 24 for the slower refracted-

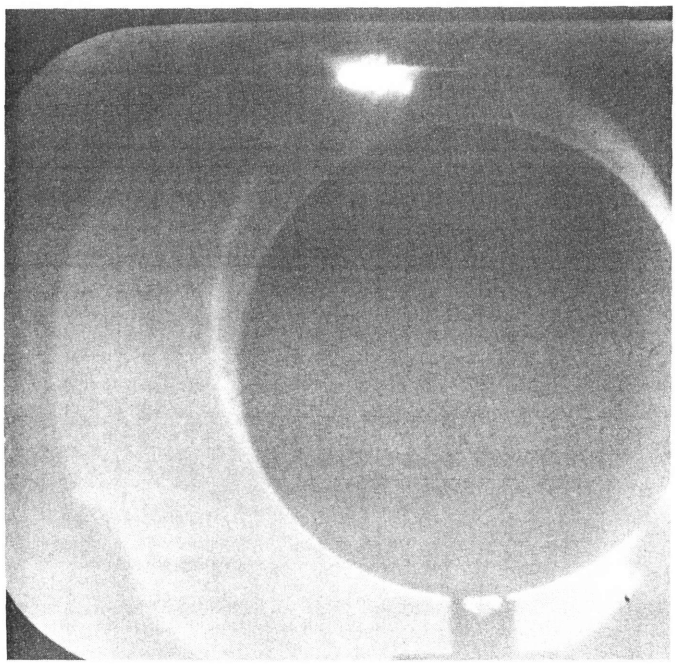

Fig. 32(a)—Schlieren photograph of the wavefront resulting from the circumferential wave generated at 15° incidence for an aluminum cylinder in water (ka = 1008).

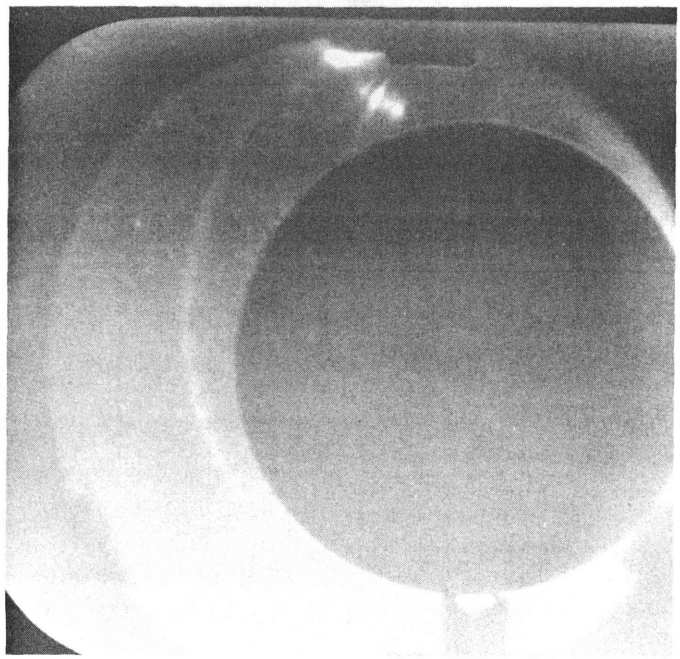

Fig. 32(b)—Schlieren photograph of the wavefront resulting from the circumferential wave generated at 15° incidence at a later time than in Fig. 32(a).

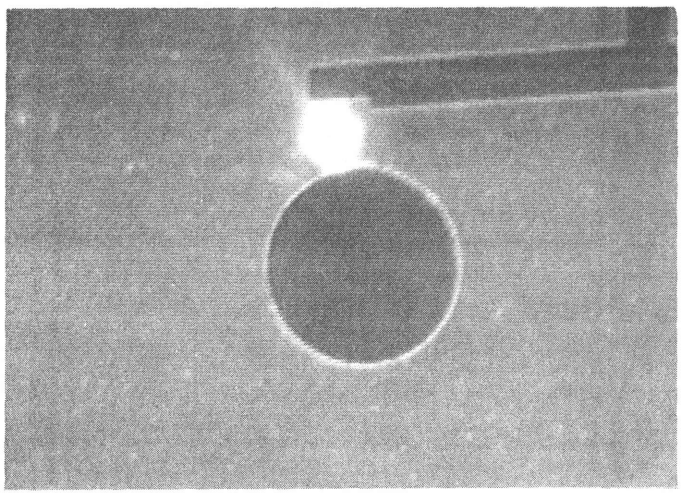

Fig. 33(a)—Schlieren photograph of the wavefront resulting from the circumferential wave generated at 15° incidence for an aluminum cylinder in water (ka = 215.8).

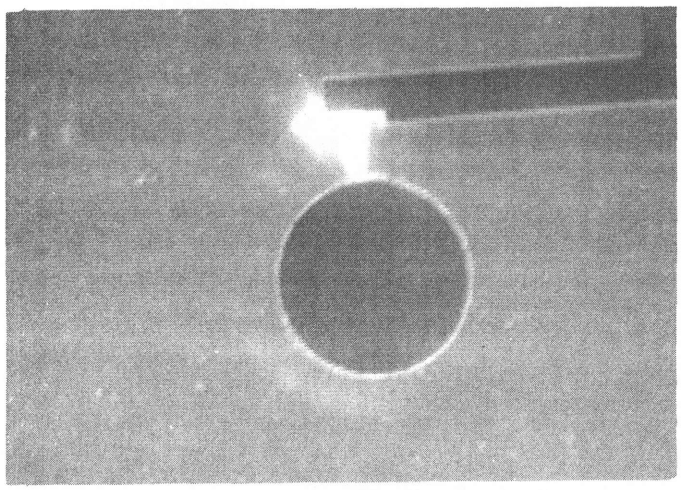

Fig. 33(b)—Same as Fig. 33(a) except at a later time.

circumferential wave is given for the wave which was generated at 15° incidence in Fig. 34. This construction yielded a value of c_c/c_w of 6.4 for two successive times which is in reasonable agreement with the hydrophone data result of 6.6 for a ka of 323.7. Figure 35 is the same sort of geometric construction for a ka of 215.8. In this case, since the

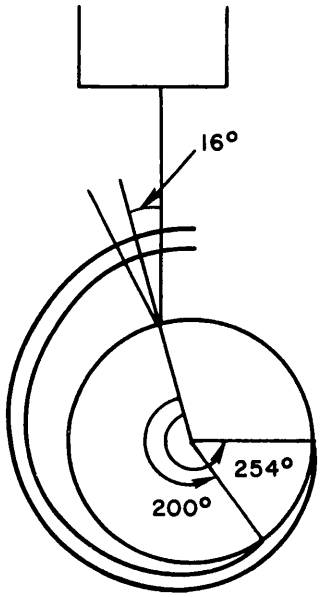

Fig. 34—Geometric construction corresponding to the Schlieren visualization of wavefronts of Figs. 31(a) and (b) at ka = 323.7.

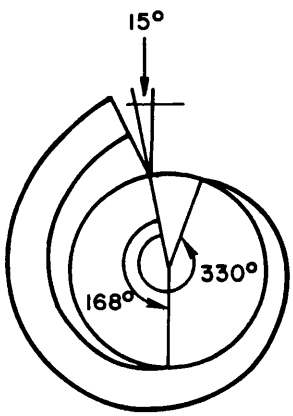

Fig. 35—A geometric construction corresponding to photographs in Figs. 32(a) and (b) (ka = 215.8).

point where the wavefront touched the cylinder surface was not visible, the wavefront had to be constructed to fit the part of the wavefront which was visible. A velocity ratio (c_c/c_w) of 6.7 was measured in this case compared to a ratio of 6.6 determined by hydrophone measurements.

For this wave the theoretical value for critical angle using Eq. 5 is 9° derived from measured wave speeds. As in the case of the slower refracted circumferential wave, the nominal experimental value, in this case 15°, is somewhat higher than the theoretical approximation predicts but is not at great variance with it.

IV – The Total Diffracted Field

Selective insonification of specific regions of the cylindrical surface have allowed the separate observation of specific types of waves which have characteristic incidence angles, circumferential speeds, and attenuations. These waves may be considered as major constituents of the total diffraction resulting from the interaction of incident acoustic energy and a cylindrical object which it encounters. Similarly any other shape such as a sphere, spheroid, etc. will cause diffraction which may be regarded as composed of separate waves in the same way, however with somewhat more complicated results than found here for a cylinder. The constituents of the total field which exist at a given time may be observed by insonification of only one half of the cylinder with a sensibly plane wave. With the plane wave incident from above, the result is shown in Fig. 36(a). A key to the Schlieren photograph is presented beside it in Fig. 36(b) in which the bracketed and labeled parts are identified as follows:

A. The illuminated portion of the cylinder surface.

B. The specularly reflected wave.

C. The Franz or creeping wave shortly after launching.

D. The refracted circumferential wave generated at approximately 30° incidence. In the same region, this wave is not separated from the radiated wave caused by the directly-transmitted shear wave resulting in a broadening of the wave front.

E. The wave resulting from the direct transmission of a compressional wave in the cylinder. This was verified by determining the equivalence of the time of travel in water, of the specular wave B on a line back toward the source and the combined time of travel of a compressional wave through the cylinder on the same line through the cylinder axis, plus the time of travel (on the same line) to the wavefront labeled E.

The radiation caused by the circumferential wave generated at approximately 15° incidence is absent in this situation because of the small degree to which it is generated relative to the other waves.

It can easily be visualized now that if a hydrophone were placed at a position such as P, indicated in Fig. 20, as all of these waves expand in time propagating away from the cylinder, a sequence of pulses would be detected. First, the wave generated at

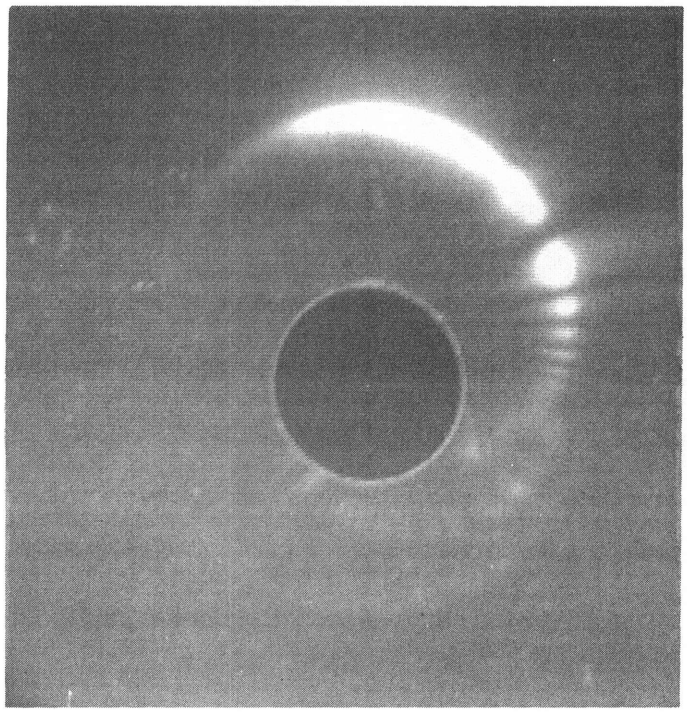

Fig. 36(a)—Schlieren photograph of the waves produced when the upper right quadrant is insonified with an incident plane wave traveling toward the bottom of the picture.

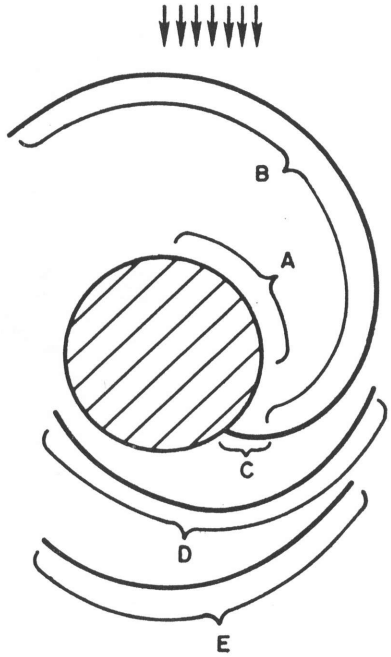

Fig. 36(b)-Diagram for interpretation of Fig. 36(a). A-Illuminated portion; B-Specular reflection; C-Franz wave; D-30° wave; E-Through compressional wave.

approximately 15° would appear. Second, the compressional wave (E) would appear; then the mixture (C) of the 30° wave and that one resulting from the shear wave in the aluminum; and finally the creeping wave (D) would be detected as it passed the hydrophone.

When the entire cylinder was insonified from above with an incident wave which was essentially plane, the Schlieren photograph of Fig. 37 resulted. Here sets of waves are

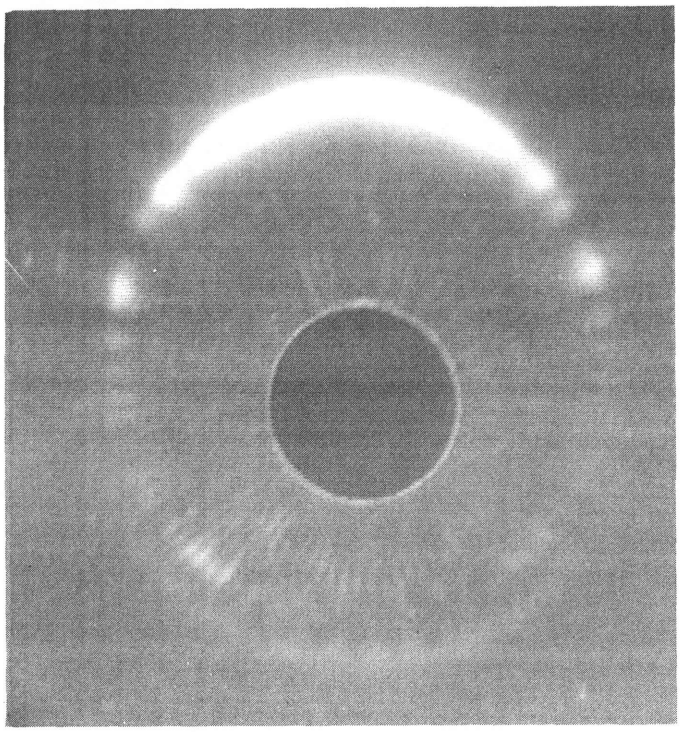

Fig. 37–Schlieren photograph of the entire diffracted field produced when the upper half of the cylinder is insonified.

generated in both directions around the cylinder causing interference between them resulting in a somewhat confused picture. However, not so confused that the reader cannot select identifiable portions of wavefronts with far less doubt than we would have had without the benefit of the pictures of the separated waves. A hydrophone placed at a point of the field on the shadow side of the cylinder would produce a very complicated pulse sequence of much larger total duration than the incident pulse.

V – A Discussion of Experimental Results and Comparison With the Calculations of Uginčius

The theoretical computation by Uginčius was carried out without the benefit of experimentally measured parameters relating to the problem such as the Lamé constants (λ, μ) or the easily related shear or longitudinal wave velocities in a readily obtainable material. The Lamé constants were handbook[26] values attributed to "rolled" aluminum, presumably pure. A reasonable approximation to pure aluminum is commercially available as aluminum type 1100 which is 99% pure aluminum. Although obtainable, this material is not readily commercially available in a reasonable variety of extruded stock sizes of circular cylindrical bars. In addition, type 1100 has the undesirable machining qualities of being very soft and "gummy". On the other hand, aluminum type 6061 (97.9% Al, 1.0% Mg, 0.6% Si, 0.25% Cr, Cu) is readily available in a variety of stock sizes and is readily machined. The consistency of the elastic properties among samples was determined by actually measuring the shear and longitudinal wave velocities in samples from the same pieces of stock of which the finished cylinders were made on which circumferential waves were measured. The shear-wave speed was ~~6370~~ 3136 m/sec and the longitudinal wave speed was ~~3136~~ 6370 m/sec. The estimated accuracy of these measurements was ± 30 m/sec. These values yield values of Lamé constants of $\lambda = 5.64 \times 10^{11}$ dyn/cm^2 and $\mu = 2.66 \times 10^{11}$ dyn/cm^2 as compared to the values assumed in the theory of $\lambda = 6.1 \times 10^{11}$ dyn/cm^2 and $\mu = 2.5 \times 10^{11}$ dyn/cm^2. Because of these differences, the experimental result may be reasonably expected to differ quantitatively in some respect with the theoretical computation. Nevertheless, the three separate waves which were observed were found to have values of velocity related to each other in the same way that the waves related to the Franz and Rayleigh-type poles in the complex ν-plane were. The Franz wave is adequately represented, for high ka, by the pole in the line of F poles which has the lowest attenuation. The Franz wave is highly attenuated. The wave which has properties which approach the properties of the plane-surface-Rayleigh wave on a water-bounded-curved surface as a limit (the R1 wave), has a speed higher than the shear or Rayleigh wave speed. Its attenuation is less than that of the Franz wave and for aluminum it is generated at an incidence angle in the neighborhood of 30°. The

third circumferential wave which seems to contribute to the total diffracted field to a significant degree is generated in aluminum at an incidence angle near 15° and is the least attenuated of the three distinct waves which were observed. Its velocity is also the highest of the three waves. It also seems to be generated to the least extent.

By means of these waves, Uginčius[13] also calculated differential scattering cross-section of infinite aluminum cylinders. The geometry of the theory is two dimensional, i.e., one dimension, the length of the cylinder, is infinite; and any real physical situation must necessarily be three dimensional. Any experimental verification must, therefore, be limited by this forced approximation which is of unknown magnitude and might easily be of the magnitude of the differences sought in the value of differential cross section with changes in ka or azimuthal angle. In the experiment, an attempt was made to minimize the error by illuminating the smallest possible length of cylinder consistent with far-field measurement and the limitations of available transducers.

Differential scattering cross section is given by Uginčius[13] as

$$\frac{d\sigma}{d\theta} = \lim_{r\to\infty} r \frac{|p_r|^2}{|p_i|^2} .$$

This formulation presumes the inverse square root diminution of pressure with the distance (r) from the cylindrical axis in the far-field of the cylinder. Here p_i is the pressure of the incident wave at the position of the cylinder in its absence, and p_r is the pressure measured at the distance (r) from the cylinder axis. Actually the pressure diminishes with r as shown in a specific case in Fig. 38 where hydrophone output voltage (proportional to pressure) is plotted versus inverse$\sqrt{r}$. The straight line through the origin contains all points which follow the inverse $\sqrt{r}$ diminution required. The points plotted are experimental measurements. A curve through these measured points is seen to reasonably approach the straight line for large r. In order to compare experimental values with computed values, a sufficiently large value of r is taken such that

$$\frac{1}{r}\frac{d\sigma}{d\theta} = \frac{|p_r|^2}{|p_i|^2} .$$

Experimentally measured points are plotted on reproductions of plots taken from Uginčius for $(2/a)\, d\sigma/d\theta\,|_{\theta}$ versus ka in Figs. 39, 40, and 41 for the values of θ of 60° 90°, and 180° respectively. The experimental points are plotted on an absolute basis

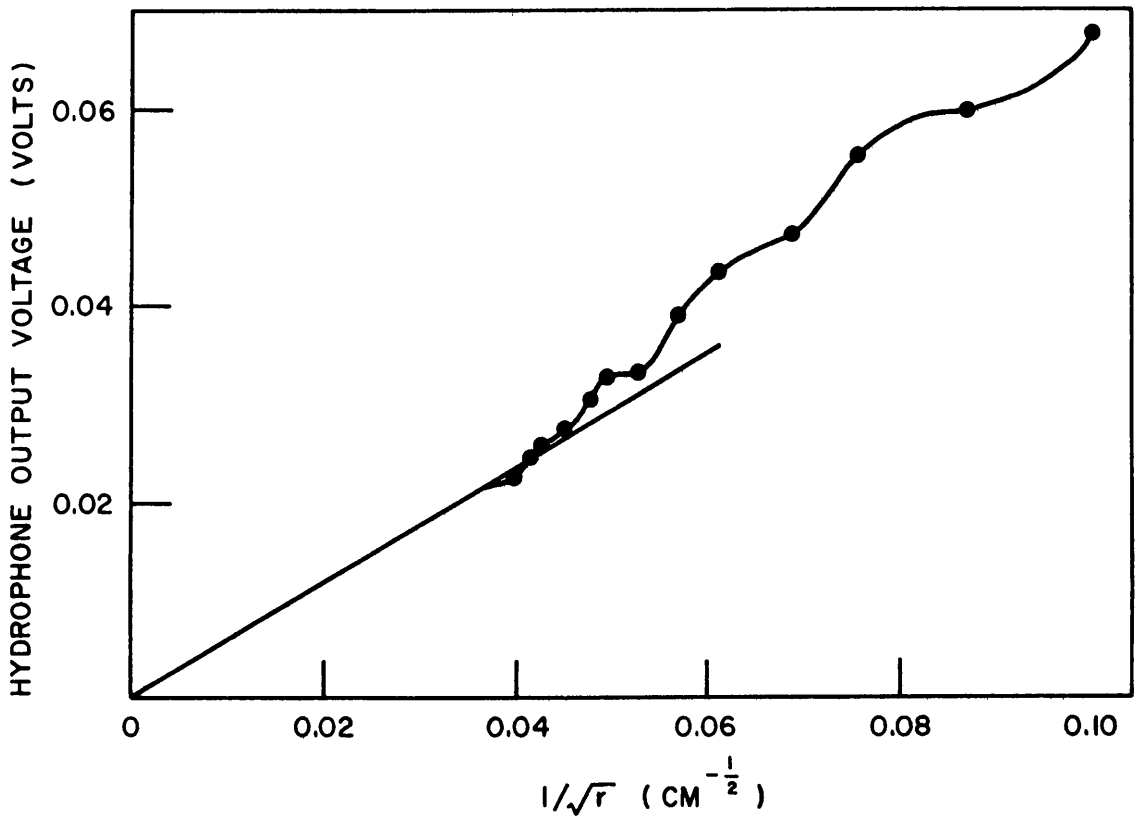

Fig. 38–Plot showing the approximate inverse $\sqrt{r}$ diminution of hydrophone output voltage.

with respect to theory. Surprisingly, considering the lack of correspondence between theoretical assumption and experimental reality, regions of considerable agreement are found especially in the case of $\theta = 90^{\circ}$ for low ka. It should be mentioned that this theory is for steady-state signals and the experiment is done with pulsed sine waves. Although the pulse extensions were long compared with the cylinder diameter, a smooth portion which could be taken to be steady state was not always available. Another limitation was at high ka when the cylinder diameter occupied a large portion of the source beam which would cause nonuniform illumination of the cylinder. This appears to be the case at high ka for $\theta = 60^{\circ}$ in Fig. 39. On the other hand, however, the data does not seem to be so affected for $\theta = 90^{\circ}$ in a similar ka range. The large changes in amplitude found in the theoretical curve over relatively small ka ranges results in extreme difficulty in detecting a stable steady-state portion of the pulse as seen

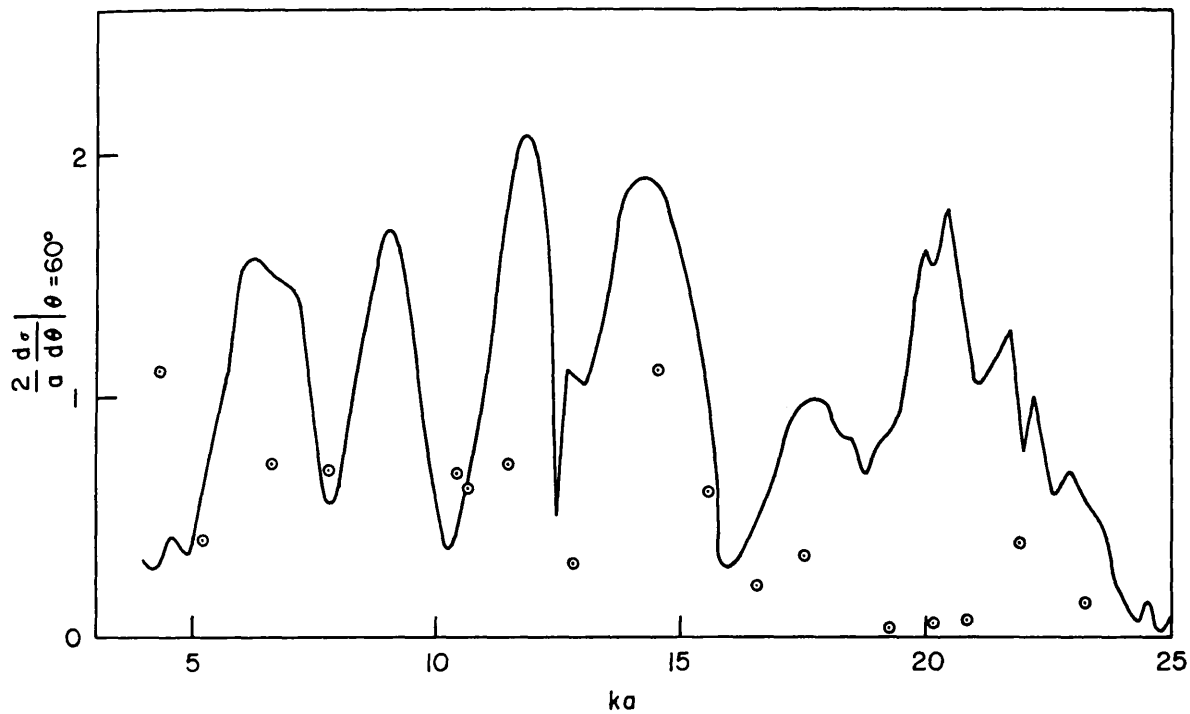

Fig. 39—Experimental measured values plotted on curves of scattering cross section vs. ka for scattering angle $\theta = 60°$ taken from the theory of Uginčius.

by the relatively poor agreement of the experimental points in such regions. In all cases, however, it is seen that the magnitudes of theory and experiment for the abcissa are in reasonable agreement. The reason that the scattering cross section measurements were made at low ka (below 25) was, as indicated above, that the entire width of the cylinder had to be illuminated uniformly and at the same time, while not at the same time illuminating the receiver directly since these assumptions were made with theoretical calculations of both Uginčius and Faran.

Measurement was also made of the angular variation of scattering cross section for the case in which Uginčius compares his calculation with that of Faran and also Faran's experimental values. Essential agreement was found with Faran's theoretical calculations as may be seen in Fig. 42(a) for an aluminum cylinder of type 4043 (95% Al). For backscattering $\theta = 180°$. Again the experimental points are plotted on an absolute scale relative to the theory. Although the same agreement is not found for type-1100

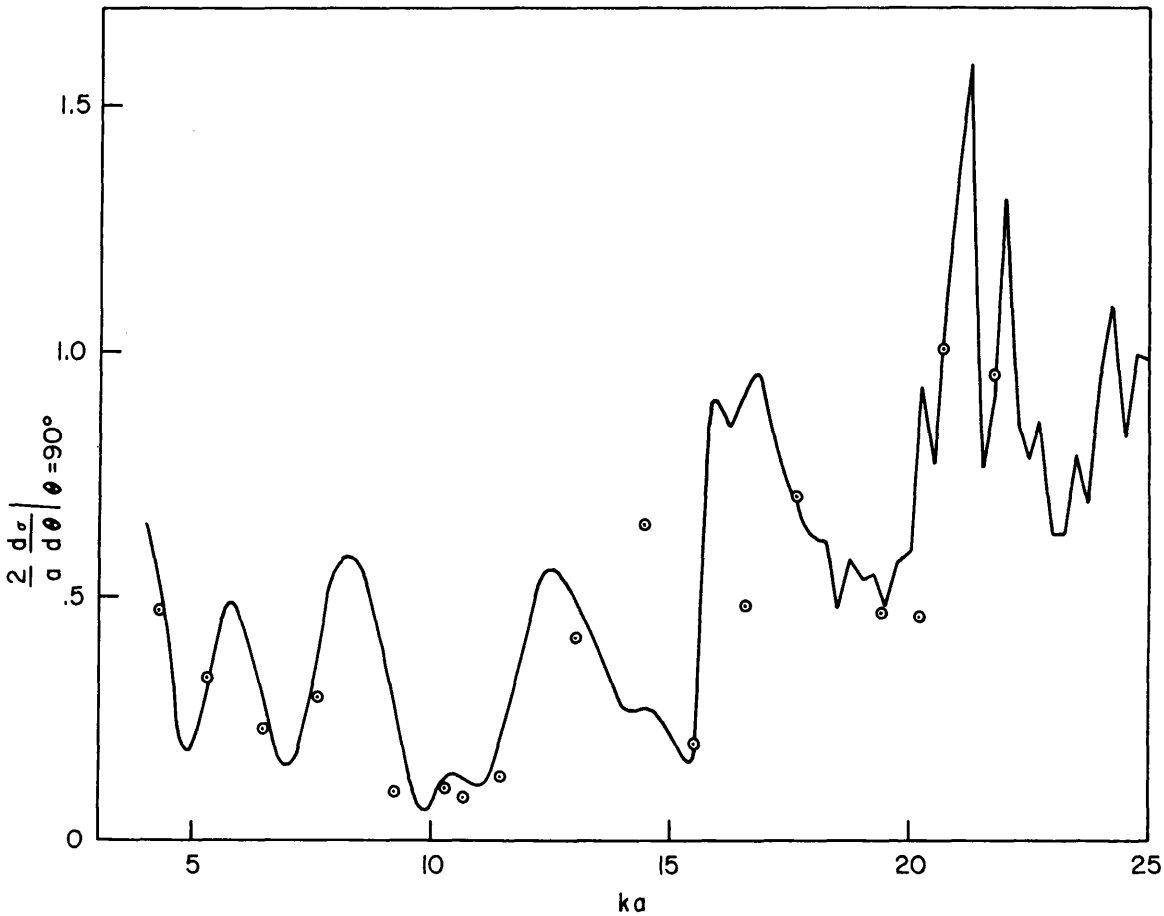

Fig. 40—Experimental measured values plotted on curves of scattering cross section vs. ka for scattering angle $\theta = 90°$ taken from the theory of Uginčius.

(99% Al) aluminum cylinder at a ka of 5, a similar deep null is found (Fig. 42(b)) at $\theta = 180°$. The significant part of these measurements was that the null at 180° found by Faran at a ka of 5 was found in these measurements also. Uginčius found the minimum point in the backscattered direction at a value of 4.78. Measurement at that ka (4.78) seen in Fig. 43 shows that indeed a less complete null exists at that ka showing some deficiency in the creeping wave calculation with respect to this calculation. This conclusion was true for two different aluminum alloys denoted type 1100 (99% Al) and type 4043 (95% Al).

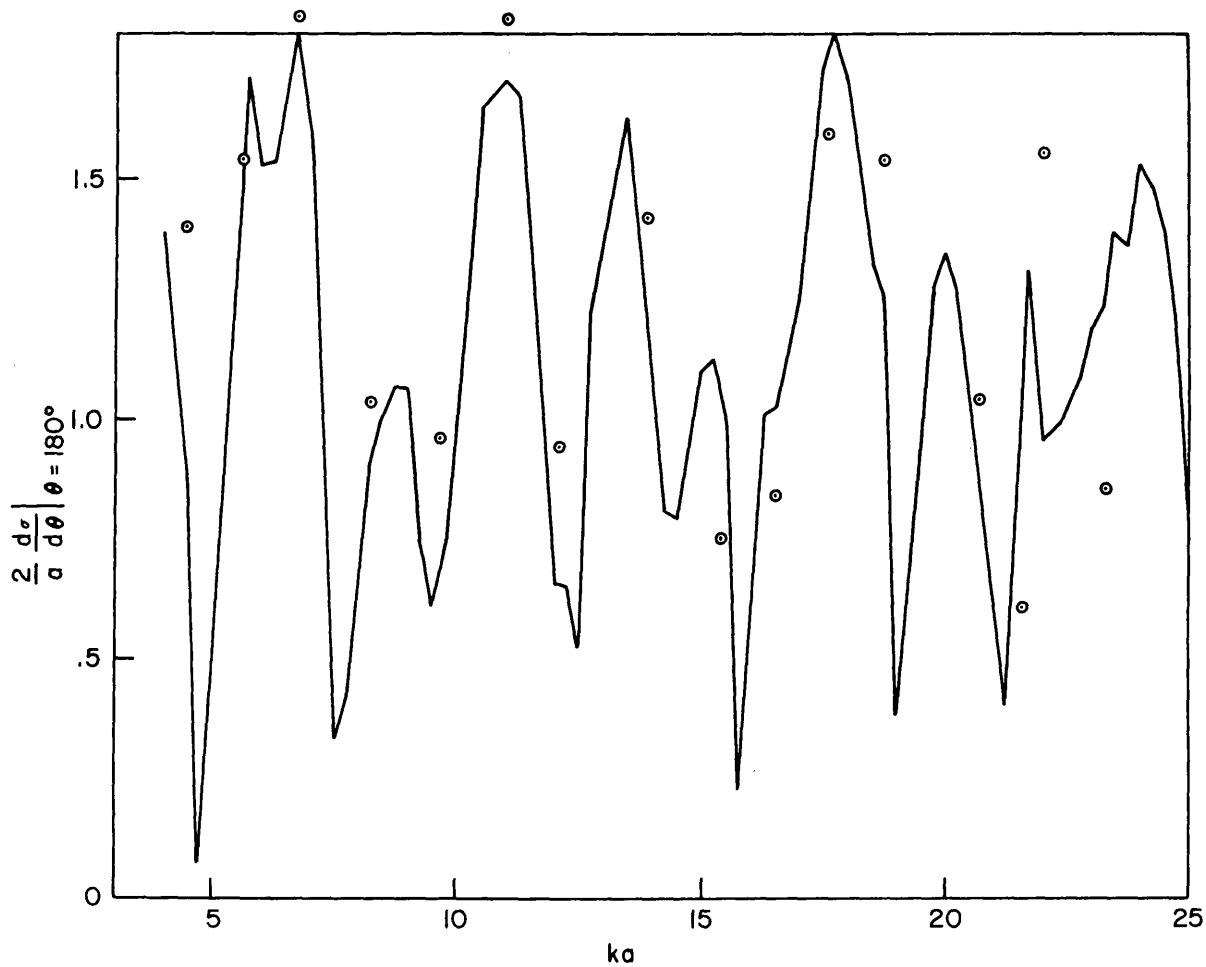

Fig. 41—Experimental measured values plotted on curves of scattering cross section vs. ka for scattering angle $\theta = 180°$ taken from the theory of Ugincius.

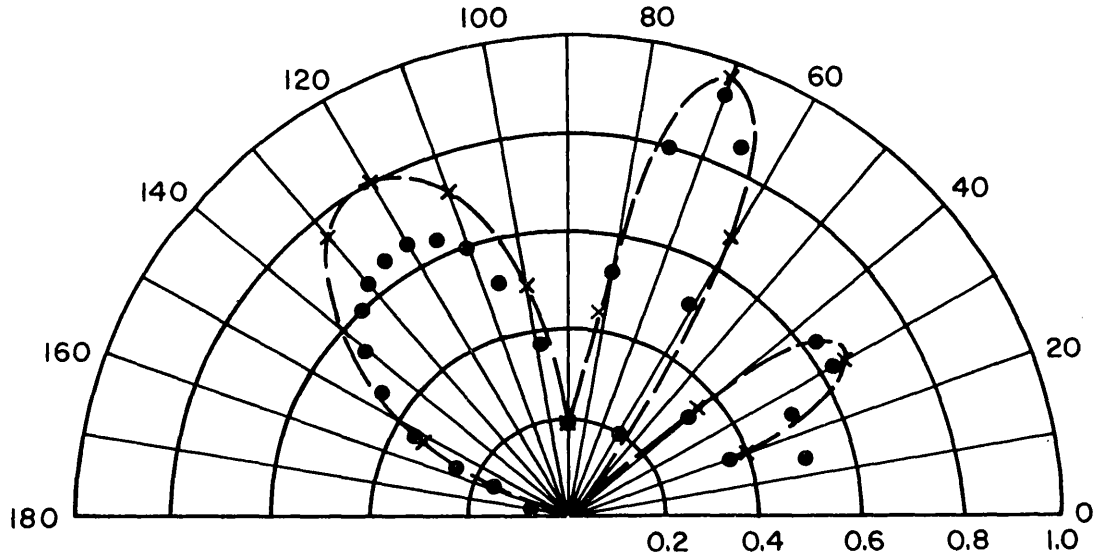

Fig. 42(a)—Experimentally measured points (·) for a 4043 Al cylinder at ka = 5 of scattering cross section vs. scattering angle θ and the comparable curve taken from the theory of Faran (×—×—).

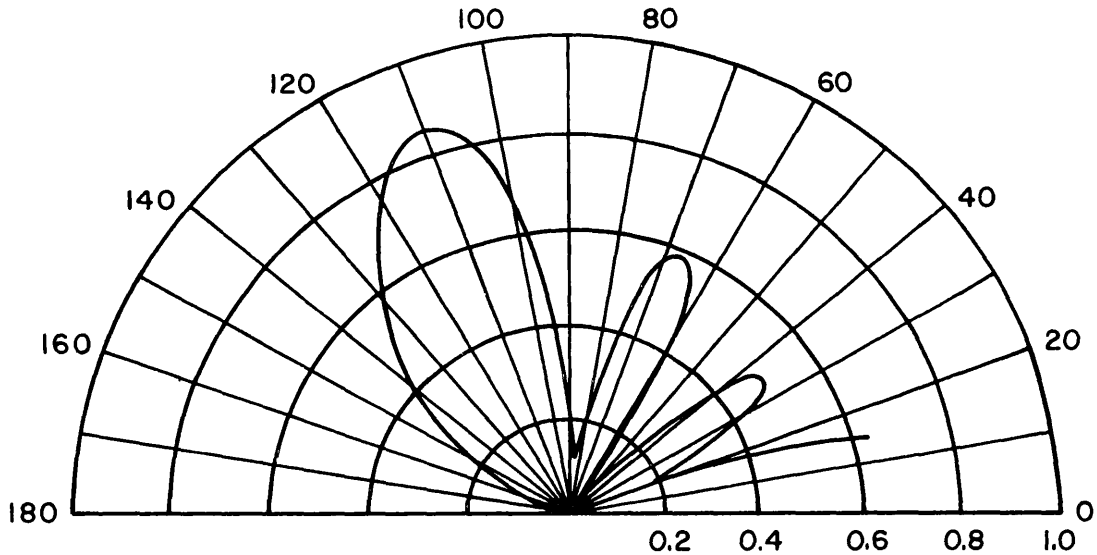

Fig. 42(b)—Experimentally measured curve of scattering cross section vs. scattering angle θ for an 1100 Al cylinder at ka = 5.

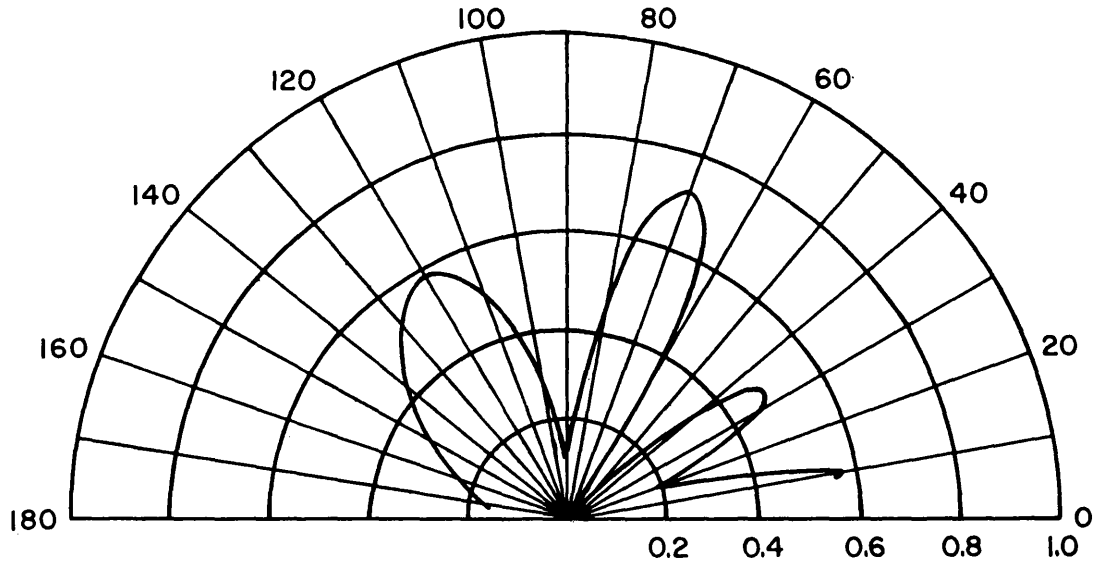

Fig. 43–Experimentally measured curve of scattering cross section vs. scattering angle θ for an 1100 Al cylinder at ka = 4.78.

VI – Conclusions

Three distinct types of circumferential waves have been observed in experiments which allowed the types of waves to be observed separately with a pulsed acoustic signal. Of major significance is the observation of the waves at all. In addition, some of the properties of the waves were determined for the case of a solid aluminum cylinder.

The "Franz" or "creeping" wave is generated at tangential incidence and travels on the external side of the cylinder surface. Its properties are primarily determined by the geometry of the diffracting or reflecting object although the elastic properties of the cylinder do influence the properties of the wave, especially the attenuation. The creeping wave is highly attenuated, in the order of 3 Np/rad. The velocity for ka's greater than 54 is only 1% lower than that of the free water-borne wave and may be computed to within less than ±0.5% by Franz's formula for the rigid case. Whereas Ugin̆cius concluded on the basis of calculations at ka = 5, that aluminum shells of $b/a < 0.75$ act as rigid with respect to the creeping wave, experimental measurements show that for higher ka (ka = 215.8) shells even with $b/a \leq 0.99$ act as rigid with respect to the creeping wave.

A refracted circumferential wave is characteristically generated at an incidence and emergence angle near 30°, travels on the inside of the cylinder boundary, and is less attenuated than the creeping wave. Its attenuation is 0.10 to 0.18 Np/rad and its speed is near 2.5 times the free water-borne wave speed. The wave properties are more directly related to the elastic properties of the surface than the curvature of the surface on which it travels. This wave has been reasonably identified as one whose properties approach the properties of the Rayleigh wave for a plane surface. It is, therefore, referred to as a "Rayleigh type" wave.

A third wave was observed which is very similar to the one generated at 30° incidence except that it is generated at an incidence and emergence angle of 15°. It also travels on the inside of the curved boundary. It is the least attenuated of the three distinct waves observed and is apparently generated to a lesser degree than the other two. Its attenuation is 0.08 to 0.14 Np/rad and its speed is much higher than the other two; 6.5 times the free water-borne-wave speed. The wave may be related to one of the higher Rayleigh-mode poles in the complex ν-plane discussed by Ugin̆cius[13].

Some experimental agreement is found with the total field calculation of Uginčius in the form of differential scattering cross section for various scattering angles over a ka range between 5 and 25. However, experimental measurements confirm the minimum point in the scattering pattern for a ka of 5 rather than at 4.78 calculated by Uginčius by the "creeping wave method." This indicates a possible shortcoming of the calculation method perhaps due to the admittedly ignored background integral. The three types of waves were measured with pulses. Values of ka ranged from 54 to 1008 with two independent experimental methods. A pressure pulse sequence was measured with a hydrophone and radiated wavefronts were observed with the Schlieren method of wavefront visualization. The two methods established the same velocities of the refracted circumferential waves stated above.

ACKNOWLEDGEMENTS

I gratefully acknowledge the encouragement and advice of Dr. H. Überall in the course of this work and also his leading position in the theoretical work which prompted these experimental investigations. I thank L. R. Dragonette for his help in taking the data.

This work was done at the Naval Research Laboratory under the Edison Memorial Training Program. For this award, I am very grateful. Most especially, thanks are extended to my supervisor Dr. R. L. Steinberger for creating and maintaining a working environment in which it was possible to carry out this investigation. I also wish to thank Mr. Henry Chaskelis for his help with the Schlieren photographs and the use of that system which he developed. The expert typing of Mrs. Donna Carpenter helped me immeasurably.

REFERENCES

1. G. N. Watson, Proc. Roy. Soc. (London) A59, 83-99, 546-563 (1919).
2. B. van der Pol and H. Bremmer, Phil. Mag. 24, 141-176, 825-864 (1937).
3. W. Franz and K. Deppermann, Ann. Phys. 10, 361-373 (1952).
4. A. Freedman, Her Majesty's Underwater Detection Establishment, U. Pamphlet Number 605, August 1958.
5. G. R. Barnard and C. M. McKinney, J. Acoust. Soc. Am. 33, 226-238 (1961).
6. C. W. Horton, W. R. King, and K. J. Diercks, J. Acoust. Soc. Am. 34, 1929-1932 (1963).
7. K. J. Diercks, T. G. Goldsberry, and C. W. Horton, J. Acoust. Soc. Am. 35, 59-64 (1963).
8. T. G. Goldsberry, J. Acoust. Soc. Am. 42, 1298-1305 (1967).
9. M. V. Mechler, Thesis, Dept. of Physics, University of Texas, Austin, Texas, 1967 (unpublished).
10. R. R. Goodman, R. E. Bunney, and S. W. Marshall, J. Acoust. Soc. Am. 42, 523-524 (1967).
11. R. Hickling, J. Acoust. Soc. Am. 36, 1124-1137 (1964).
12. H. Überall, R. D. Doolittle, and J. V. McNicholas, J. Acoust. Soc. Am. 39, 564-578 (1966).
13. R. D. Doolittle and H. Überall, and P. Uginčius, J. Acoust. Soc. Am. 43, 1-14 (1968).
14. P. Uginčius and H. Überall, J. Acoust. Soc. Am. 43, 1025-1035 (1968).
15. I. A. Vikterov, Rayleigh and Lamb Waves (Plenum Press, New York, 1967).
16. L. M. Brekhovskikh, Sov. Phys. – Acoust., 13, 462-472 (1968).

17. A. J. Rudgers, Paper A6 presented at the Seventy-Fifth Meeting of the Acoust. Soc. Am. (1968).

18. J. J. Faran, Jr., J. Acoust. Soc. Am. 23, 405-418 (1951).

19. P. Wille, Acustica 15, 11-25 (1965).

20. R. E. Bunney, Thesis, Dept. of Physics, Colorado State University, Fort Collins, Colorado, 1968 (unpublished).

21. O. D. Grace and R. R. Goodman, J. Acoust. Soc. Am. 39, 173-174 (1966).

22. W. Franz, Z. Naturforsch 9a, 705-716 (1954).

23. J. B. Keller, J. Appl. Phys. 28, 426-444 (1957).

24. A. Freedman, Acustica 12, 61-70 (1962).

25. F. G. Friedlander, Sound Pulses (Cambridge University Press, London, 1958) p. 152.

26. W. P. Mason, American Institute of Physics Handbook, (McGraw-Hill Book Co., New York, 1957).

27. W. G. Neubauer, J. Acoust. Soc. Am. 34, 312-318 (1962).

28. W. G. Neubauer and L. R. Dragonette, J. Acoust. Soc. Am. 36. 1685-1690 (1964).

APPENDIX A

The Experimental Apparatus and Procedures

The acoustic data taken by means of a hydrophone which sensed the pressure of an acoustic wave were all taken in one of two water tanks suitably instrumented for the purpose. One which had a capacity of approximately 250 gallons was built to the standards of a normal aquarium of that size. The walls were 1/2 in. plate glass and the bottom was a single slab of slate. Its dimensions were 30 in. x 72 in. x 30 in. deep. A frame was placed on top of the tank which allowed the positioning of acoustic sources, receivers, and cylinders. A side view of the tank showing the frame and the positioning of transducers and cylinders in the water is shown in Fig. A1. A top view showing the means of

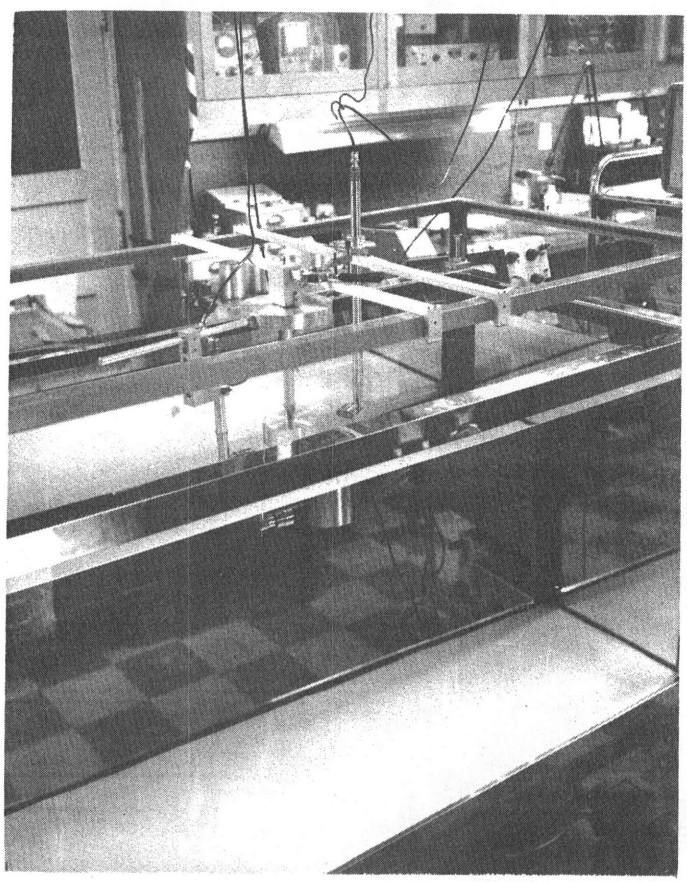

Fig. A1—A side view of the glass-walled tank showing the framework which supported the transducers and diffracting cylinder.

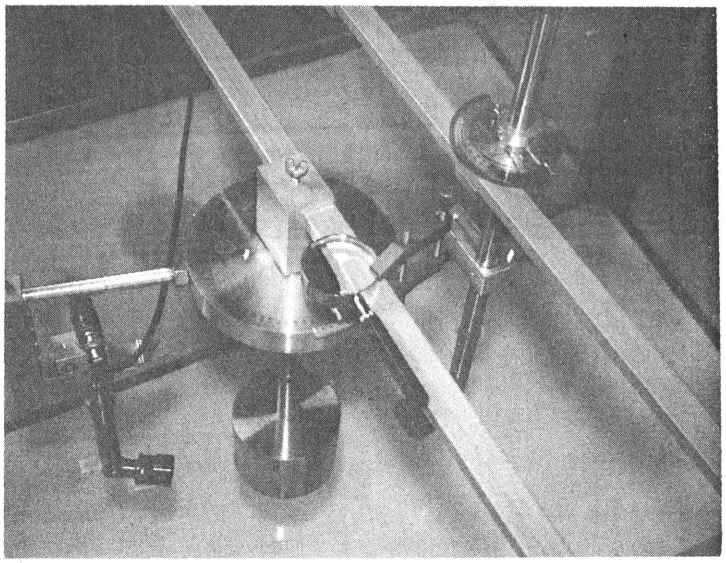

Fig. A2—A top view of the experimental apparatus in the glass-walled tank. The source is on the right, a 4 in. aluminum cylinder is mounted in the center, and the hydrophone is on the left.

mounting and the normal relative positions of acoustic source, receiver, and aluminum cylinder may be seen in Fig. A2. For a specific series of measurements, the source is fixed at a position on the rail which spans the longitudinal frame members. Means were provided for rotating the source to a position usually established by maximizing the desired acoustic signal at the hydrophone. The source could then be locked in any position. The diffracting cylinder was rigidly mounted on a shaft on which a drum, whose perimeter was graduated in degrees, was free to rotate about the cylinder axis. A shaft extending radially from the drum was slotted to receive the hydrophone bracket. On this bracket, the hydrophone was permitted to rotate and be locked in any desired position. Thus the hydrophone could be rotated about the diffracting cylinder axis and also be oriented, relative to the cylinder surface, at any position.

For precise and accurate measurement of velocity and attenuation especially for the Franz wave, two rods were attached, by a fixture below the drum, to the shaft which held the diffracting cylinder so that these rods would rest on top of the sides of the tank. The rods had a screw adjustments where they rested on the tank so that the cylinder and hydrophone combination could be titled transversely with a very fine adjustment. Also,

a fixture on the cylinder shaft allowed a rod to be clamped, near the water surface between the shaft and the acoustic source support rod. This allowed the parallelism between cylinder surface and source face to be carefully adjusted and once established, rigidly fixed. These features were necessary in order to insure the measurement of a wave which traveled around the circumference rather than a spiral path which would yield a wave speed smaller than the correct speed assuming a circumferential path derived from the radius of the cylinder. Also, they insured that the weight of the hydrophone and its bracket did not cause the cylinder position to shift relative to the position of the source. With these precautions and with a 0.1° vernier on the graduated drum, which was read through a magnifying glass seen clamped to a rail in Fig. A2, an accuracy of ±0.5% was achieved for the values of velocity of the Franz wave. On the other hand, such consistantly high accuracy was not possible for attenuation measurements because of the necessity of measuring the signal amplitude over the wide range of amplitude of the Franz-wave signal. The accuracy of attenuation ranged smoothly between ±0.9% for the 2.54-cm (smallest) diameter cylinder and ±5.4% for the 15.24-cm (largest) diameter cylinder.

In order to measure time differences accurately, the position of the acoustic pulse was measured on the time scale of a 20-MHz sine wave from which the pulse imposed on the acoustic source was ultimately generated. A 20-MHz sine wave was generated by a Hewlett Packard Frequency Synthesizer. Displayed with this signal on successive sweeps of the same oscilloscope was a one MHz signal generated from the same source and, therefore, synchronous with it. The 20-MHz signal was also scaled down by a factor of 10^5 making a pulse also synchronous with it. The amplified output of the pulse generator was impressed on the source transducer. The acoustic pulse was observed on the oscilloscope screen and its location relative to the following one MHz peak was determined by counting 20-MHz peaks to the next peak of the one MHz peak. A drawing of the oscilloscope display is shown in Fig. A3. When the path length of the acoustic signal was increased, the acoustic signal would advance, in time, relative to the background of 20 and one MHz peaks. The number of one MHz peaks which the acoustic pulse passed as the path was increased were counted and recorded. When the desired angular position for the hydrophone was reached, the number of 20 MHz peaks to the last passed one MHz peak were counted. The total number of peaks thus counted gave the time difference due to the path increase around the cylinder circumference, at least to the nearest half cycle of 20 MHz, or 0.025 μsec.

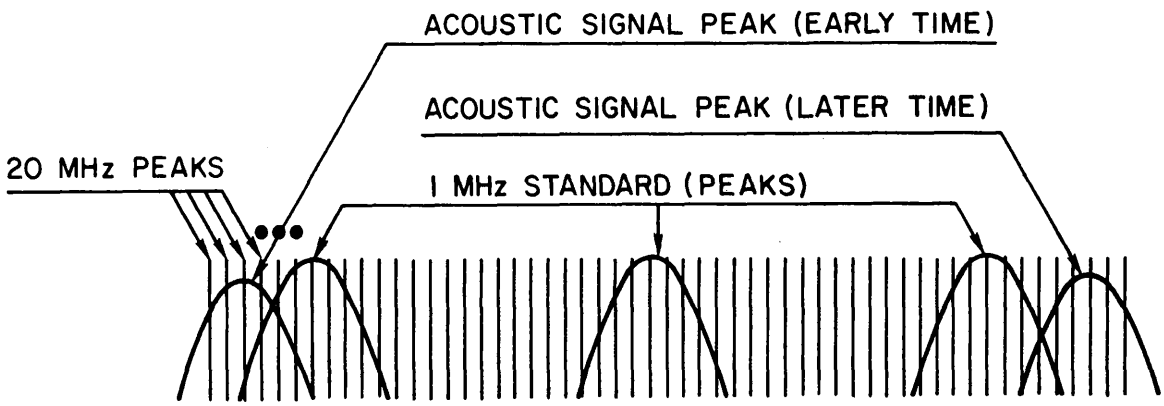

Fig. A3—A drawing of the appearance of the oscilloscope-tube face when one and 20 MHz were used to determine accurate time differences.

In obtaining values for attenuation, the lack of precision and accuracy was not due to the inherent difficulty of measuring the amplitude of a transient signal with an oscilloscope. This difficulty was overcome by alternately adding to and subtracting from the pulse signal, an accurately established dc voltage which would bring the pulse-signal peaks (positive and negative respectively) to the same reference point on the oscilloscope face. The accurate dc voltage then represented the amplitude of the pulse. In this way, the major limitation of cathode-ray tube face non-linearity was avoided. The limiting factor in determining the amplitude of the signal was the nature of the acoustic signal itself. In all cases of the refracted type of circumferential wave, there was a significant background of interfering pulses. These background pulses are coherent with the signal pulse. Differences in path between the desired and undesired pulse of only a half wave-length would cause amplitude changes in the desired pulse of twice the amplitude of the background pulse. It was not possible, therefore, to determine the circumferential-wave attenuation with desired accuracy. In the case of the Franz wave at high ka, the pulse was not in the presence of any significant background pulses and the attenuation values are directly related to the measurement of parameters of time and path differences and are, therefore, much more accurate than for the refracted-circumferential waves.

The relatively small glass-sided tank was used for measuring the circumferential-pulse sequences. No pulses reflecting from the side walls interfered with the desired pulses in most cases. If and when such wall pulses did exist, they were identified and avoided. The glass tank was too small to allow a sufficient distance between the cylinder

and hydrophone at all angles around the cylinder so the scattering-cross-section experiments were done in a larger tank which has been previously described[27]. A photograph of the large tank is shown in Fig. A4. The tank has 3 in. thick cypress walls and bottom containing a water volume 5 ft x 10 ft x 5 ft deep. Locations of acoustical elements in a

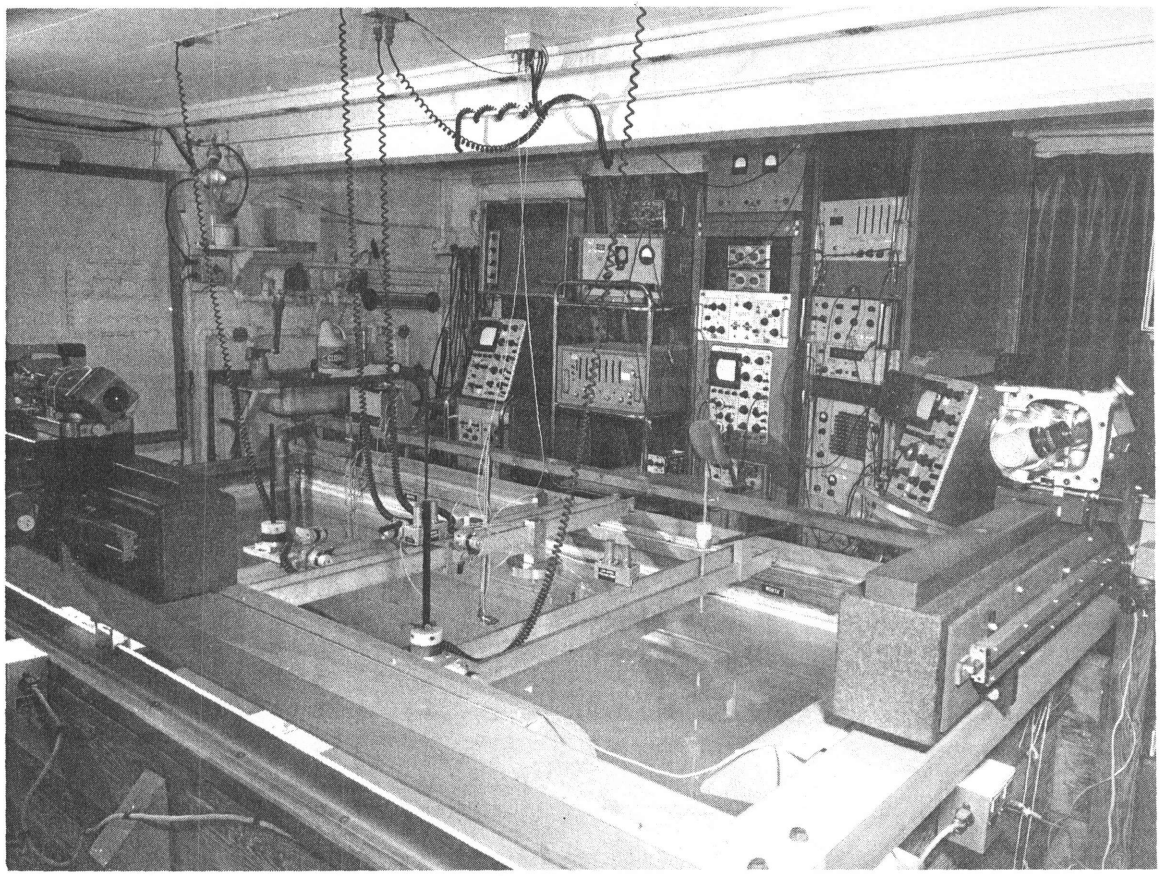

Fig. A4—A view of the large wooden tank showing the placement and location equipment on top of the tank.

volume one-meter square by 10-cm deep in the center of the tank's volume is accomplished optically with microalignment telescopes mounted at right angles to each other on two sides of the tank and a vertical cathetometer which views through a porthole in one end of the tank. Elements are placed in the tank by a system of tracks, rails, and carriages mounted on top of the tank. The scattering-cross-section measurements were made at a frequency of 200 KHz. The hydrophone was the one described earlier with a sensing disc

of 0.160 cm diameter. A more detailed description of this hydrophone and details of its construction may be found in Ref. 25. A truncated sine-wave pulse-generating system was also used for these measurements. The block diagram of this system is given in Fig. A5. At times this system was also used in order to get a more desirable pulse shape

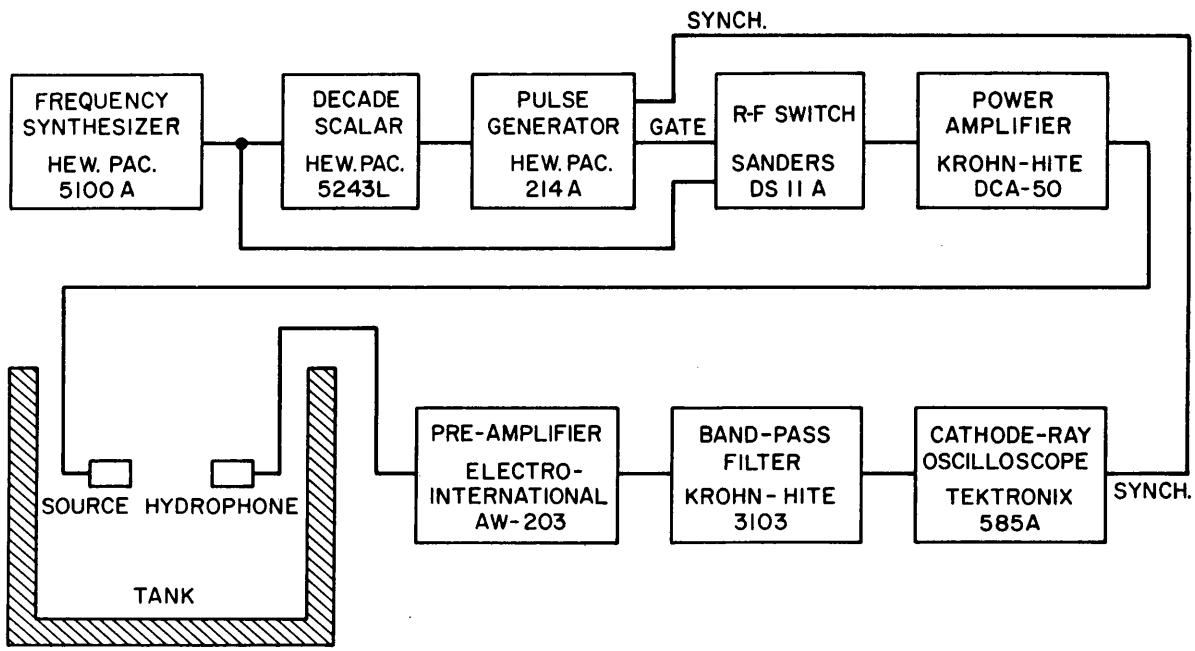

Fig. A5—Block diagram of the truncated-sine-wave-pulse-generation system.

for some of the measurements other than those of scattering cross section. For the most part though, the source pulse was produced with a simpler pulse-generator and amplifier system whose block diagram is shown in Fig. A6. In order to get an accurate value of the free water-borne-wave speed (c_w) used to express circumferential-wave speed as a ratio, the temperature of the ambient water was measured and values taken from tables of sound speed previously determined by Neubauer and Dragonette[28] in the larger of the two tanks.

Unfortunately, the lowest ka for which it was possible to measure circumferential waves meaningfully was a value of 54. At lower ka no adequate source transducer was available. In addition, below ka = 54 the pulse sequence of circumferential and all other waves become very confused. The Franz-wave path was so short that an impractically short pulse was required to separate it from the refracted-circumferential and through-waves in the cylinder. This circumstance unfortunately leaves a gap between the highest

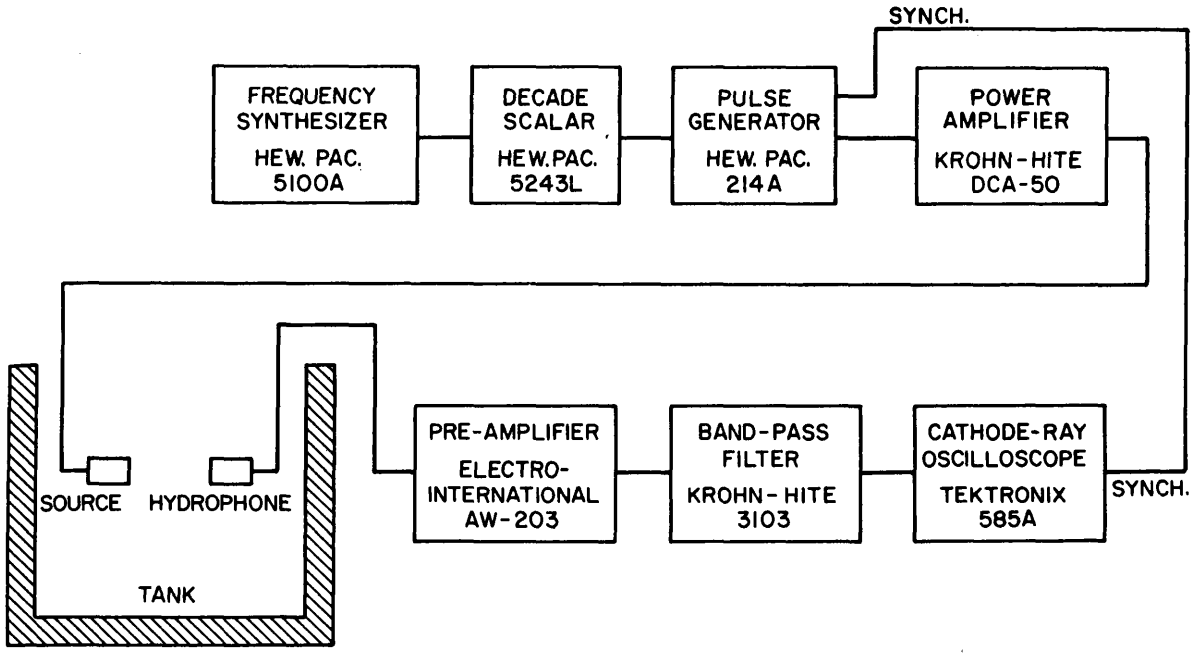

Fig. A6—Block diagram of the pulse system used when the acoustic source was driven with a step function or short, single polarity pulse allowing the source to ring at its resonant frequency producing a pulse as shown in Fig. 2.

value of ka = 25 for which Uginčius calculated and the lowest ka = 54 for which experimental measurements were made for the Franz wave on an aluminum cylinder.

APPENDIX B

The Schlieren Visualization of Waves

Since the classical Schlieren method was used extensively throughout this work, a qualitative description of the method and apparatus will be presented. The illustration in Fig. B1 shows the elements sufficient to produce a Schlieren image. The Schlieren method

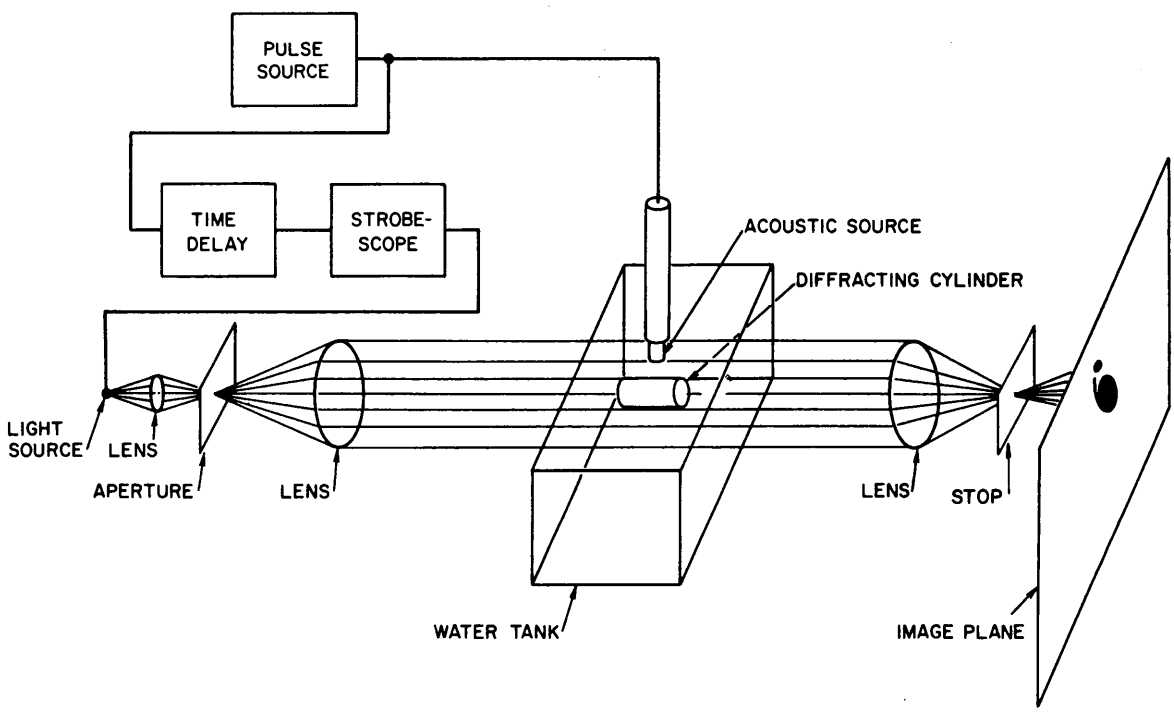

Fig. B1—A schematic diagram of a system for Schlieren visualization of acoustic waves.

is effectively a means for increasing the contrast in order to be able to view a low contrast object. With a pulsed-light source, a parallel beam is produced between the two large lenses. The light is focused at a point at which a stop is placed essentially nullifying the parallel beam. In the parallel beam is placed a transparent tank which does not destroy the parallelism of the beam and contains water. Sound is generated in the tank

and made to propagate in a direction normal to the parallel-light beam. The change of index of refraction in the water due to the acoustic pressure wave causes rays in the parallel-light beam to be refracted so that essentially the stop is ineffective for those rays and an image is formed on a screen or film behind the stop. The effect is to eliminate the constant background of parallel rays in the beam and view the desired effect in the image plane. In order to observe circumferential waves on cylinders, the cylinder is placed in the water normal to the sound beam with the cylinder's surface elements aligned parallel to the light beam. The acoustic source is pulsed and strobescopic light is triggered with an appropriate delay to illuminate the acoustic pulse at some point in its propagation.

In this system used in this study, the image behind the optical stop was imposed on a television iconoscope and displayed on a closed-circuit-television monitor. This permitted a considerable degree of adjustment to optimize the image for showing those features desired. Photographs of the television screen resulted in the pictures shown in this work.

This page intentionally left blank.

Security Classification

DOCUMENT CONTROL DATA - R & D

(Security classification of title, body of abstract and indexing annotation must be entered when the overall report is classified)

1. ORIGINATING ACTIVITY *(Corporate author)* Naval Research Laboratory Washington, D.C. 20390	2a. REPORT SECURITY CLASSIFICATION Unclassified 2b. GROUP

3. REPORT TITLE

THE EXPERIMENTAL EXAMINATION, BY MEANS OF PULSES, OF CIRCUMFERENTIAL WAVES ON ALUMINUM CYLINDERS IN WATER

4. DESCRIPTIVE NOTES *(Type of report and inclusive dates)*

An interim report on one phase of the problem.

5. AUTHOR(S) *(First name, middle initial, last name)*

Werner G. Neubauer

6. REPORT DATE November 15, 1968	7a. TOTAL NO. OF PAGES 70	7b. NO. OF REFS 28

8a. CONTRACT OR GRANT NO. NRL Problem S01-04 b. PROJECT NO. RF 05-511-401-5252 c. d.	9a. ORIGINATOR'S REPORT NUMBER(S) NRL Report 6791 9b. OTHER REPORT NO(S) *(Any other numbers that may be assigned this report)*

10. DISTRIBUTION STATEMENT

This document has been approved for public release and sale; its distribution is unlimited.

11. SUPPLEMENTARY NOTES	12. SPONSORING MILITARY ACTIVITY Dept. of the Navy (Office of Naval Research) Washington, D.C. 20360

13. ABSTRACT Three types of waves which contribute to the total acoustic diffracted field of an aluminum cylinder in water are isolated by generating each wave to the exclusion of the other two. Observations of circumferential propagation speed and attenuation are made. The "Franz type" or "creeping" wave is generated separately on the outside of aluminum cylinders with ka ranging from 54 to 1008. The circumferential-wave speed is found to be 1% less than that of the free water-borne wave in agreement with the theory for a rigid cylinder. The attenuation of these waves on aluminum cylinders is significantly less than the theory for the rigid cylinder predicts. Another circumferential wave with approximately a 30° incidence and emergence angle is found to propagate on the inside of the curved boundary. This wave has an attenuation ranging between 0.10 and 0.18 Np/rad and has a speed of 2.5 times that of the free water-borne wave. This is classified as a "Rayleigh type" wave. A third wave is observed which is similar to the wave generated at 30° incidence but has a 15° incidence and emergence angle. The attenuation is between 0.08 and 0.14 Np/rad and has a speed of 6.5 times that of the free water-borne wave. Experimental measurements of differential-scattering cross section are compared to those calculated by means of the creeping wave formulation.

DD FORM 1 NOV 65 1473 (PAGE 1)

S/N 0101-807-6801

Security Classification

14. KEY WORDS	LINK A		LINK B		LINK C	
	ROLE	WT	ROLE	WT	ROLE	WT
Sound						
Acoustic properties						
Circumferential waves						
Cylinders						
Creeping waves						
Sound diffraction						

DD FORM 1 NOV 65 1473 (BACK)
(PAGE 2)